DEVELOPMENT OF RADAR ALTIMETRY DATA PROCESSING IN THE OCEANIC COASTAL ZONE

ESA/ESRIN Contract No. 21201/08/I-LG (CCN 3)

Deliverable on

GPD global implementation

Version 1.1

Code	COASTALT-D2.1c-1.1	**Edition**	1.1	**Date**	05-08-2011
Client	European Space Agency	**Final User**		-	

	Name	Signature	Date
Written by	UPorto (Joana Fernandes, Clara Lázaro, Alexandra Nunes, Miguel Salgado)		05/08/2011
Approved by			
Revised by			
Authorised by			

DISSEMINATION	COPIES	MEANS
ESA, Jérôme Benveniste, Salvatore Dinardo and Bruno Lucas	1	Electronic
NOCS, Paolo Cipollini	1	Electronic

SUMMARY OF MODIFICATIONS

Ed.	Date	Chapter	Modification	Author/s
1.1	05/08/2011	1.2.4	"P(hs)" for "P(h0)"	J. Fernandes
1.1	05/08/2011	2.2	"GN-S" for "GNSS" in the caption of table 3	J. Fernandes
1.1	05/08/2011	2.3	"were" for "where", "covariance" for "correlation" on text, caption of figure 15 and caption of table 4; "COV" for "COR" on the header of table 4	J. Fernandes
1.1	05/08/2011	3.1	Apart from the first paragraph, text has suffered major modifications, replacing the reference to the initial by the present global implementation; Figures 21 to 24 have been updated	J. Fernandes
1.1	05/08/2011	3.2	The text has been changed to describe the latest results; Figures 25 and 26 have been updated; Four new figures (27 to 30) have been added to illustrate the results.	J. Fernandes
1.1	05/08/2011	3.3	Field mwr_rejection_flag replaced fields radio_landocean_flag and mwr_qua_interp_flag; description of field GPD_interp_flag was updated	J. Fernandes
1.1	05/08/2011	4.0	The last two paragraphs have been updated	J. Fernandes

TABLE OF CONTENTS

Reference Documents

[RD1] **COASTALT Project Management Plan v1.3,** COASTALT2-PMP-13, February 7, 2011

[RD2] **Wet Tropospheric Corrections in Coastal Areas**, COASTALT Deliverable D2.1b v1.2, 30/06/2009

[RD3] **Global assessment of GNSS-derived tropospheric corrections**, COASTALT CCN3 Deliverable D2.1a v1.1, 26/07/2010

Acronyms

2T - 2-meter Temperature
AC - Analysis Centre
CPU – Computer Processing Unit
ECMWF - European Centre for Medium-range Weather Forecasts
EPN - EUREF Permanent Network
ESA – European Space Agency
F-PAC – French Processing and Archiving Facility
GMF - Global Mapping Functions
GNSS - Global Navigation Satellite System
GPD - GNSS-derived Path Delay
IGS - International GNSS Service
MJD – Modified Julian Date
MWR - MicroWave Radiometer
NaN – Not a Number
NMF – Niell Mapping Functions
PPP - Precise Point Positioning
RADS - Radar Altimeter Database System
RD1 – Reference Document 1
RD2 – Reference Document 2
RD3 – Reference Document 3
RINEX - Receiver INdependent EXchange format
SGDR - Sensor Geophysical Data Record
SLA – Sea Level Anomaly
SLP - Sea Level Pressure
SurfP- Surface pressure
TB – Brightness Temperature
TB23 – Brightness Temperature at the 23 GHz channel
TCWV - Total Column Water Vapour
UPorto - University of Porto
VMF1 - Vienna Mapping Functions 1
ZHD - Zenith Hydrostatic Delay
ZTD - Zenith Total Delay
ZWD – Zenith Wet Delay

Introduction

This document presents the Deliverable D2.1c for the COASTALT project, CCN 3, CONTRACT No. 20698/07/I-LG and is delivered for fulfilment of milestone M12.

The present report describes the work that has been done at University of Porto (UPorto) concerning the global implementation of the GNSS-derived path delay (GPD) wet tropospheric correction for coastal altimetry.

The document is divided in four sections. Section 1 introduces and describes the datasets used throughout the document. Section 2 presents the global assessment of the GNSS-derived zenith wet delay (ZWD) fields, a complement of Deliverable D2.1a. Section 3 presents the work related with the GPD global implementation. The main conclusions are summarized in section 4.

1 Datasets

1.1 Introduction

The aim of the present report is to present the studies conducted at UPorto on two main topics:

- assessment of the GNSS-derived zenith wet delays (ZWD) at global scale
- GPD global implementation

This study has been conducted using various datasets that will be described in this section. These include:

- GNSS (Global Navigation Satellite System) derived tropospheric delays from UPorto solutions using the GAMIT software and ZTD solutions available online, from the International GNSS Service (IGS) and EUREF Permanent Network (EPN)
- ECMWF (European Centre for Medium-range Weather Forecasts) global grids of several surface atmospheric parameters
- Envisat altimetry data from the Radar Altimeter Database System (RADS)

The period of analysis adopted in this study is from 1 January 2002 to 31 December 2009, from now on just referred as 2002-2009. Whenever applicable, a global analysis has been performed, that is the study region comprises the whole coastal regions covered by the Envisat satellite.

1.2 GNSS tropospheric fields

1.2.1 Dataset 1 - GNSS-derived tropospheric delays from UPorto 2010 solutions

UPorto ZTD solutions have been computed for a global set of 52 stations chosen according to the criteria described below.

The main characteristics of this processing are:

- Period: [2002 - 2009]
- Software used – GAMIT (Herring et al., 2006)
- 30-second phase measurements were used, processed using double differences
- IGS precise satellite orbits and clock parameters have been used
- atmospheric parameter estimation interval - 30 min (interpolated to 15 min interval using the *metutil* GAMIT routine)

- cut-off elevation angle - 7 degrees
- Mapping Functions used – VMF1 (Boehm and Schuh, 2004)

In the selection of the sites a set of criteria has been carefully considered, in order to choose a set of stations covering the various levels of variability of the most relevant atmospheric and oceanic conditions.

GNSS station selection criteria:

1- station location at a distance from the sea below 10 km

2- belong to IGS Reference Frame

3- possess a meteorological station

4- station location close to altimetry ground tracks

5- station location in regions with large variability in the atmospheric pressure and humidity.

A total number of 52 sites were chosen (19 EUREF, 33 IGS). From these, 46 are coastal sites with a distance from the coast < 10 km and are represented in Figure 1.

1.2.2 Dataset 2 - ZTD solutions from IGS and EPN

Both IGS and EPN provide online ZTD solutions, which have been compiled for a large number of stations (487). From these, a set of 127 coastal stations with distance to the coast less than 20 km, orthometric height less than 1000 m and that do not belong to dataset 1, were selected and are represented in Figure 2.

Both IGS and EUREF adopt processing strategies which in various aspects are different from the UPorto processing. The IGS and EPN datasets were already described in [RD3]. Below only the main aspects of the adopted processing methodologies in each of the centres are summarised.

IGS PROCESSING of ZTD ("IGSnew" solutions) (Kouba, 2009)

- These solutions are available from 2000 onwards
- software used: Gipsy (Zumberge et al., 1997) using PPP (Precise Point Positioning) with IGS Final orbits/clocks
- atmospheric parameter estimation interval - 5 min
- cut-off elevation angle - 7 degrees
- mapping functions – NMF (Niell, 2001) used until March 2009; GMF (Boehm et al., 2006) from there onwards.

EUREF PROCESSING of ZTD

- software used – Bernese (Dach et al., 2007)
- atmospheric parameter estimation interval – 1 hour
- cut-off elevation angle - between 3 and 15 degrees (3 in the majority)

- Mapping Functions – NMF and GMF (NMF in the majority)

In the EUREF processing three epochs are identified with changes introduced to the processing: GPS weeks 1133 (23 September 2001), 1319 (17 April 2005) and 1400 (4 November 2006). These changes are mainly related to the sampling interval, the a priori models and the mapping functions used for ZHD and ZWD. The major change occurred in 4 November 2006.

To evaluate the consistency between the UPorto and IGS/EPN tropospheric delays these have been compared for the common set of 51 stations of dataset 1. For these stations the mean, standard deviation, minimum and maximum of the differences between UPorto and IGS/EPN ZTD were 2.9, 5.2, 70.2, 76.0 mm respectively, for the whole period 2002-2009. Considering only the period from 5 November 2006 to 31 December 2009 these differences reduce to 0.0, 4.4, 55.8 and 70.9 mm.

1.2.3 Dataset 3 – Merged set of GNSS- derived tropospheric delays from UPorto 2008 solutions and IGS/EUREF

In 2008 UPorto computed a set of ZTD solutions for a network of stations most of them located in Europe. These solutions were available for the period 2002-2007. The stations from this dataset which do not belong to dataset 1, represented in Figure 2, were complemented with online ZTD solutions for the years 2008 and 2009.

The main characteristics of the UPorto 2008 processing are:

- Period: [2002 - 2007]
- Software used – GAMIT (Herring et al., 2006)
- 30-second phase measurements were used, processed using double differences
- IGS precise satellite orbits and clock parameters have been used
- atmospheric parameter estimation interval - 60 min (interpolated to 15 min interval using the *metutil* GAMIT routine)
- cut-off elevation angle - 7 degrees
- Mapping Functions used – VMF1 (Boehm and Schuh, 2004)

Considering the three described datasets a total of 190 coastal stations were selected with ZTD (and derived ZWD) solutions.

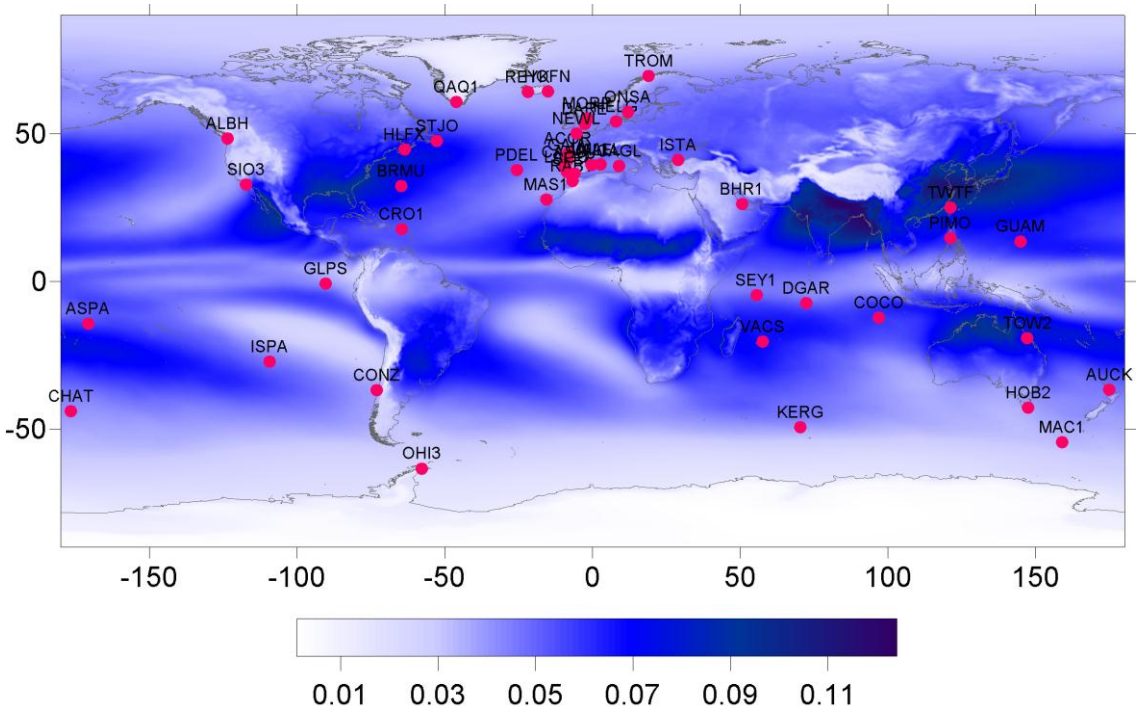

Fig.1 – Location of the network of 46 coastal stations used in the UPorto 2010 GNSS solutions (Dataset 1). The colour scale represents the ZWD standard deviation in meters.

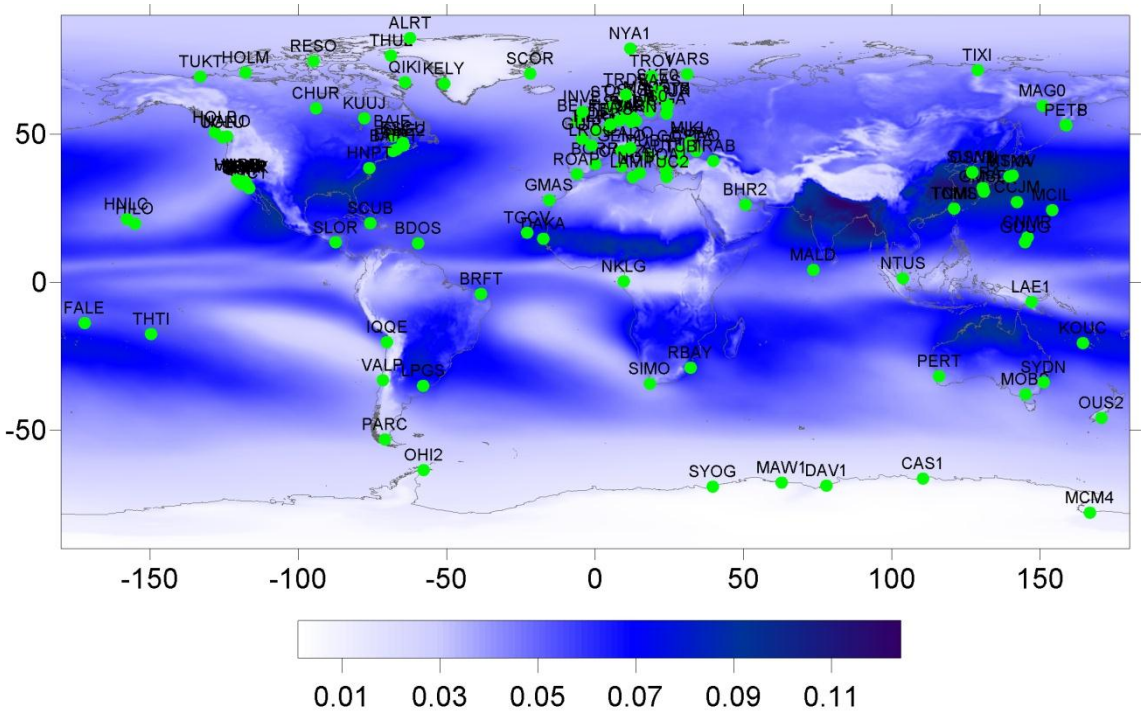

Fig.2 – Location of the network of 127 coastal stations from IGS and EPN online solutions (Dataset 2). The colour scale represents the ZWD standard deviation in meters.

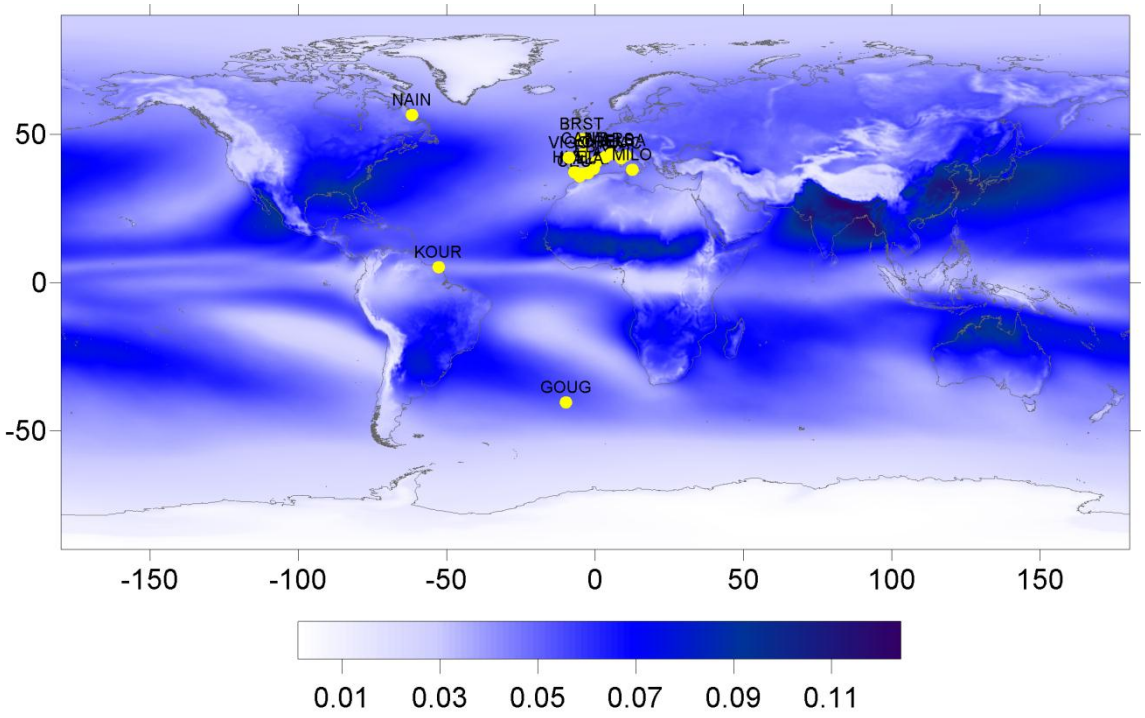

Fig.3 – Location of the network of 17 coastal stations from merged UPorto and IGS/EPN online solutions (Dataset 3). The colour scale represents the ZWD standard deviation in meters.

1.2.4 *ZWD computation*

According to the results presented in [RD3], ZTD values from the UPorto solutions with an associated GAMIT error estimate for the ZWD field larger than 20 mm and daily solutions with data gaps were discarded. The same selection criterion cannot be applied to the IGS/EUREF dataset since these online solutions do not provide any associated error estimate.

For the three described datasets of ZTD, the ZWD at sea level has been computed using the following procedure:

i) From sea level pressure, $P(h_0)$, to pressure at station height, $P(h_S)$, (Kouba, 2008):

$$P(h_S) = \frac{P(h_0)}{1-0.000022768*(h_0-h_S)^{5.225}} \quad (1)$$

ii) From pressure at station height, $P(h_S)$, to ZHD at station height (Davis et al., 1985):

$$ZHD(h_S) = \frac{-0.000022768P(h_S)}{1-0.0000226\cos(2\varphi)-0.28x10^{-6}h_S} \quad (2)$$

iii) From ZTD to ZWD at station height:

$$ZWD(h_S) = ZTD(h_S) - ZHD(h_S) \quad (3)$$

iv) From ZWD at station height to ZWD at sea level (Kouba, 2008):

$$ZWD(h_0) = ZWD(h_S)e^{\frac{h_S - h_0}{2000}} \quad (4)$$

where h_S, h_0 and φ are station ellipsoidal height, geoid height and geodetic latitude respectively. $P(h_0)$ is the sea level pressure from ECMWF global grids.

As described in [RD3] this is the most appropriate method to derive ZHD at the GNSS stations, at global scale, separate ZTD into the dry and wet component and make the altitude reduction to sea level. For each station and epoch, sea level pressure is computed from the two closest ECMWF grids, by bilinear interpolation in space and linear interpolation in time.

1.3 ECMWF global grids of several atmospheric parameters

ECMWF provides global 0.25°×0.25° grids of several atmospheric parameters every 6 hours (ECMWF, 2009). In the scope of this study, the atmospheric fields of four single-level parameters of the Deterministic Atmospheric Model were obtained for the period [2002 – 2009] and for the whole globe:

- Sea level pressure (SLP)
- Surface pressure (SurfP)
- Surface temperature (2-meter temperature, 2T)
- integrated water vapour (Total Column Water Vapour, TCWV)

1.4 Envisat Altimetry

For the purpose of comparing the wet tropospheric correction derived from the Microwave Radiometer (MWR) onboard the Envisat satellite with the corresponding GNSS-derived ZWD, altimeter data have been selected from a well known database: RADS.

For this purpose, data were extracted assuring that all 1 Hz ocean measurements are kept. These are the measurements for which the altimeter land/ocean flag is set to 0.

When using RADS to extract data for coastal altimetry studies, attention must be paid to the fields specified as default corrections used in the construction of the Sea Level Anomaly (SLA) field. For example, if the GOT4.7 (Ray, 1999) global tide model is used to compute the SLA, a number of points along the coast will be rejected, if the points with non valid SLA field are cleaned (in the RADS output file these fields appear with a NaN value). This happens because the GOT models are provided at 0.5° x 0.5° grids, as illustrated in Figure 4. As a consequence, all points shown in red in the mentioned figure will be rejected.

To avoid this, for this study RADS extraction was performed only using the altimeter land/ocean flag and keeping all points with a value 0 for this flag, even if some of the remaining extracted fields possess NaN values. In this way, we assure that there is no data loss in the coastal regions.

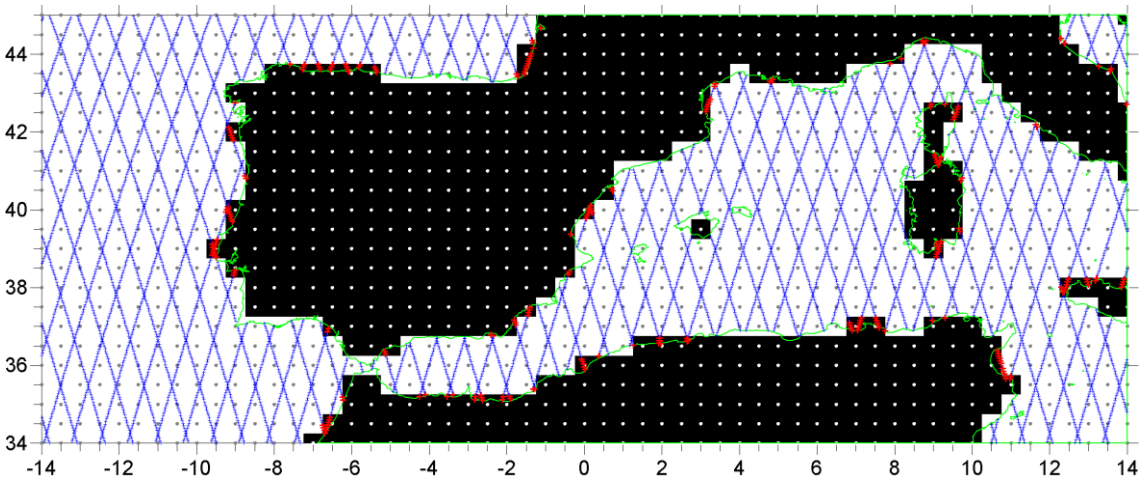

Fig.4 – Illustration of the behaviour of the GOT4.7 tide model in the coastal regions of SW Europe. Black/White dots over a white/black background represent valid/invalid nodes, respectively, of the model grids (0.5° x 0.5°). Blue and red points show Envisat 1 Hz measurements which have a valid and invalid GOT4.7 tide correction, respectively.

As already mentioned in [RD2], concerning the MWR-based wet tropospheric correction, the following updates are performed in RADS:

- at the beginning of Cycle 51, the Envisat MWR processing at F-PAC (French Processing and Archiving Facility) includes a side-lobe correction. This is intended to better model land contamination in the side lobes. The product containing the corrected TBs has been provided to RADS by ESA and has been incorporated, for cycles up to 50. For cycles 51 onwards this effect is already included in the Envisat GDRs. So, in RADS this effect is applied to all cycles in a consistent way;
- in RADS a drift correction to the TB23 is also applied: $TB23' = TB23 + 0.156 \cdot t \ (K)$, where t is time in years since 19 October 2002. The wet tropospheric correction is then recomputed using the corrected TB (TB23').

Envisat data (all required MWR-related parameters) were extracted from RADS without data loss near the coast as explained above, for the period [2002 – 2009]. Altimeter data were stacked. That is, values were interpolated into points along reference tracks. This is required to create time series of MWR fields for comparison with the GNSS-derived wet tropospheric corrections at the nearby coastal stations.

2 Global assessment of GNSS-derived ZWD fields

2.1 Introduction

The major aim of this section is to perform a global assessment of GNSS-derived wet tropospheric fields (ZWD) by extending the regional study already performed in COASTALT phase 1 and described in [RD2]. In addition, after the knowledge acquired since then, partially already reported in [RD3], the methodology adopted in this study will undergo some changes.

Although the initial aim was just to compare the GNSS-derived tropospheric fields with the MWR-derived wet tropospheric correction, during this task the need for additional studies became evident. These include the comparison with ECMWF-derived ZWD and methodologies to filter the MWR data.

2.2 Comparison between GNSS-derived and ECMWF-derived ZWD

This section describes the comparison between the GNSS-derived ZWD fields with the corresponding fields computed from the ECMWF model.

For this purpose, for each GNSS station and epoch, the corresponding ECMWF-derived ZWD was computed as follows. At each ECMWF grid node, ZWD at sea level is computed using the following procedure:

i) Using the two ECMWF single level parameters Total Column Water Vapour (TCWV) and surface temperature (2-meter temperature, T_0), the ZWD at ECMWF orography level ($ZWD(h_S)$) is computed (Askne and Nordius, 1987):

$$ZHD(h_S) = -\left(0.101995 + \frac{1708.08}{T_m}\right) * \frac{\mathrm{TCWV}}{1000} \qquad (5)$$

where T_m is the mean temperature of the troposphere, modeled from T_0 according to Mendes (2000):

$$T_m = 50.440 + 0.789 * T_0 \qquad (6)$$

ii) From the ZWD at ECMWF orography the ZWD at sea level is obtained, (Kouba, 2008):

$$ZWD(h_0) = ZWD(h_S)e^{\frac{h_S - h_0}{2000}} \qquad (7)$$

where h_S and h_0 are the ellipsoidal height of ECMWF orography and geoid height, respectively, at each grid node.

In the period 2002-2009 there were two changes in the ECMWF orography. The first occurred at 6 h of 25 November 2002 (MJD=52603.75), the second at 6 h on 1 February 2006 (MJD=53767.25). Therefore in the above reduction three different orography grids were used.

Tables 1, 2 and 3 present the statistics of the comparison for the three datasets referred above:

Dataset 1: UPorto GAMIT-derived tropospheric fields for the period 2002-2009

Dataset 2: IGS/EUREF online ZWD for the period 2002-2009.

Dataset 3: Merged solutions of UPorto GAMIT-derived tropospheric fields for the period 2002-2007 and ZWD from IGS/EUREF online solutions for the period 2008-2009.

Overall there is a very good agreement between the ZWD derived from the GNSS path delays and the corresponding value determined from ECMWF. The mean difference has an absolute value less than 3 mm and the standard deviation is 13 mm. Considering the whole set of 190 stations, the mean difference has values between -23 mm and 8 mm. Three stations have a mean difference with an absolute value larger than 20 mm and 12 stations larger than 10 mm. The standard deviation of the differences has values between 4 and 30 mm. Twelve stations a have standard deviations larger than 20 mm.

These results are illustrated in Figures 5 to 11. Figures 7 and 8 represent two typical plots of stations on regions of low temporal variability (CASC) and high variability with strong seasonal signal in the ZWD field (ESCU). Figure 9 shows the results for the station with the highest standard deviation (30 mm, LAE1). Figures 10 and 11 illustrate the behaviour of station GUAM which possesses the largest absolute mean difference (-23 mm). No relation can be identified between the position of the stations and the largest mean differences. Some occur in regions of large mean ZWD field but a few are located in regions with a small value of the mean ZWD field, for example at extreme latitudes.

As expected, the majority of the stations which possess the largest sigma values are located in regions with large variability in the ZWD field.

The results presented in tables 1 to 3 show that for some stations, the extreme values of the differences can be quite large, greater than 10 cm for many stations. Figure 11 shows a typical behaviour where it is evident the smoother ECMWF field when compared to the GNSS-derived path delay.

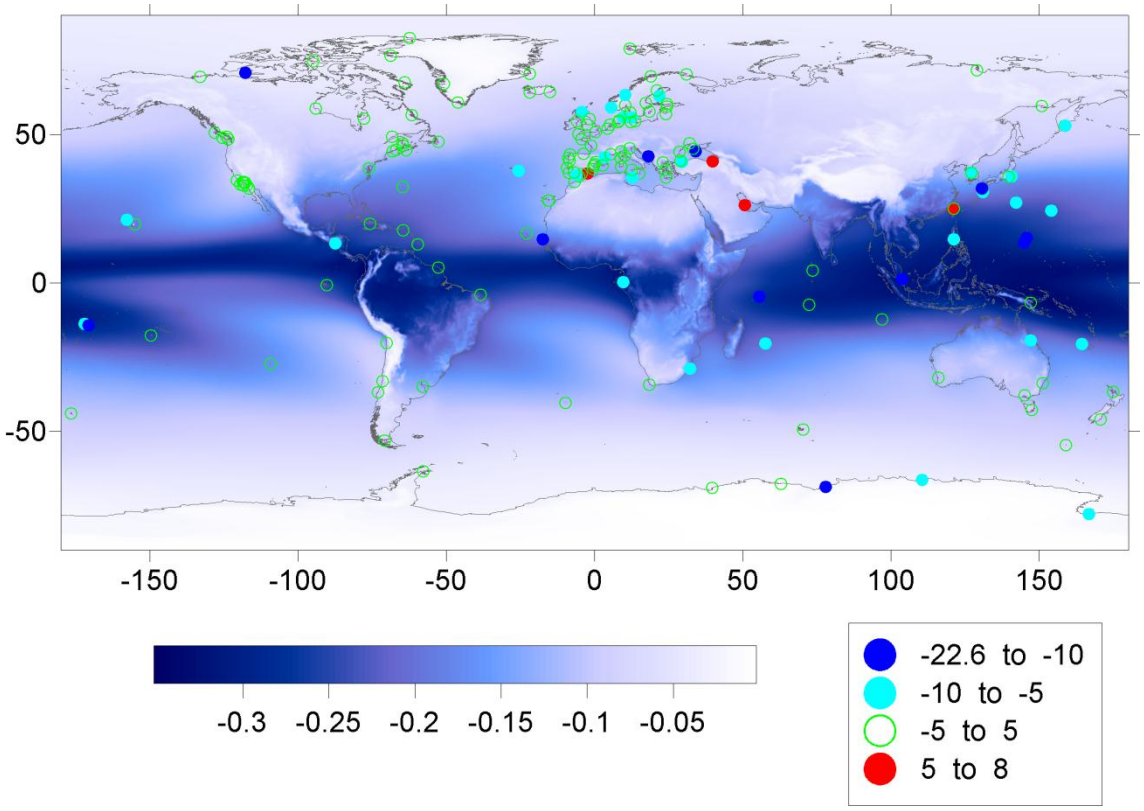

Fig.5 – Location of the full set of 190 coastal stations with available ZWD solutions. The station colour represents classes of the mean difference between GNSS-derived and ECMWF-derived ZWD at each station, in mm. The background colour scale represents the ZWD mean field in meters.

-

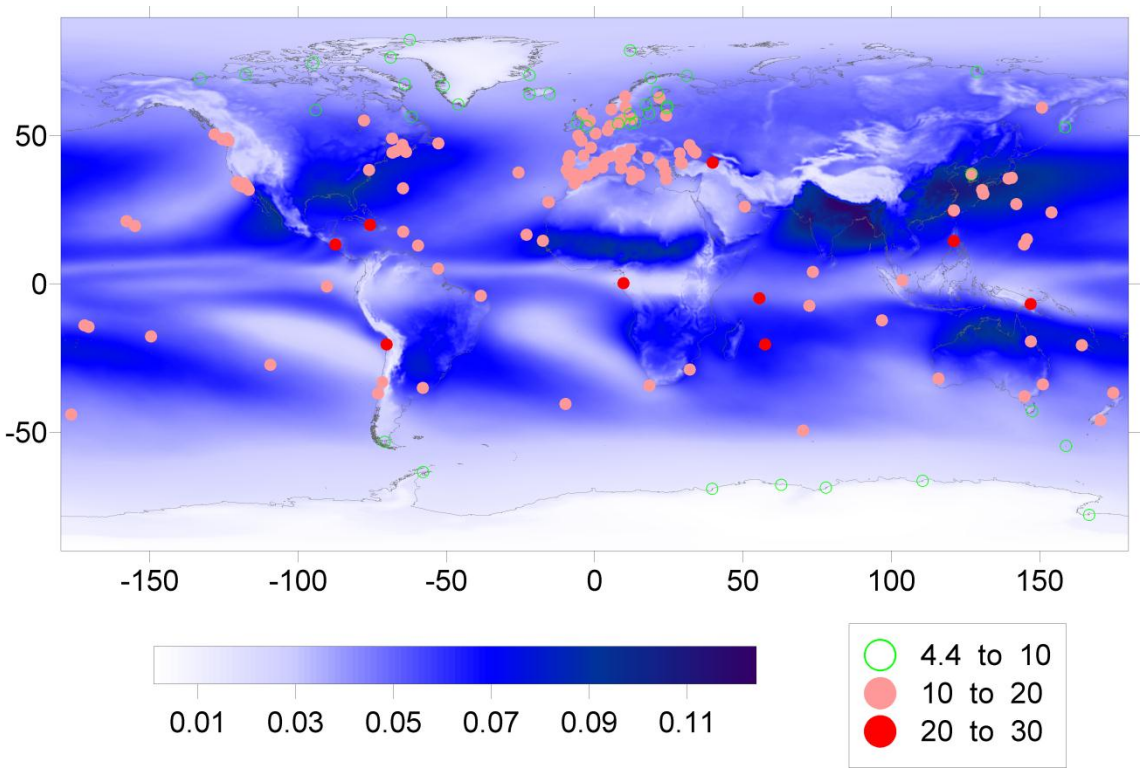

Fig.6 – Location of the full set of 190 coastal stations with available ZWD solutions. The station colour represents classes of the standard

deviation of the difference between GNSS-derived and ECMWF-derived ZWD at each station, in mm. The background colour scale represents the standard deviation of the ZWD field in meters.

Tab.1 – Statistics (mean, standard deviation, minimum and maximum) of the differences between GNSS-derived and ECMWF-derived ZWD for the 46 coastal GNSS stations of Dataset 1, for the period 2002-2009.

SITE NAME	NPOINTS	LAT (º)	LON (º)	HORT (m)	MEAN (mm)	SIGMA (mm)	MIN (mm)	MAX (mm)
ACOR	253094	43.36	-8.40	11.9	-1.2	10.7	-89.3	79.9
ALBH	276774	48.39	-123.49	50.9	3.2	11.5	-86.6	99.1
ASPA	249530	-14.33	-170.72	22.6	-11.4	17	-119	88.3
AUCK	276762	-36.60	174.83	98.3	-3.3	12	-110.5	70.9
BHR1	266295	26.21	50.61	10.7	7.5	14.8	-97.8	121.3
BRMU	255002	32.37	-64.70	23.0	-1	14.5	-122.4	117.5
CAGL	244078	39.14	8.97	192.0	-3.6	13.6	-85.9	71.4
CASC	268621	38.69	-9.42	23.0	-0.2	12.3	-93.4	76.6
CHAT	275359	-43.96	-176.57	48.1	-1	10.1	-84.2	73.2
COCO	263811	-12.19	96.83	4.8	-0.5	15.8	-100.5	107.1
CONZ	254752	-36.84	-73.03	161.1	-3.9	13.5	-95.1	83.6
CRO1	259175	17.76	-64.58	13.5	4.7	17.8	-108.4	97.2
DARE	212855	53.34	-2.64	36.6	-1.5	9.9	-78.4	72.5
DGAR	188921	-7.27	72.37	9.8	1.8	18.5	-121.9	140.8
GAIA	257241	41.11	-8.59	232.3	-4.1	13.1	-92.2	83.4
GLPS	210758	-0.74	-90.30	6.0	-1.6	12	-80.9	104.6
GUAM	265043	13.59	144.87	147.3	-22.6	21	-174	89.2
HELG	271407	54.17	7.89	9.4	-2	9.7	-77.4	68.8
HLFX	240967	44.68	-63.61	25.0	1.8	12	-101	98.3
HOB2	270434	-42.80	147.44	44.8	3.8	9.7	-80.2	93.7
HOFN	269871	64.27	-15.20	18.1	0.2	8.5	-90.1	71.2
ISPA	190712	-27.13	-109.34	117.7	-3.7	13.5	-87.2	95.8
ISTA	220389	41.10	29.02	110.1	-5	11.7	-82	56.9
KERG	262537	-49.35	70.26	33.2	-0.6	10.6	-106.4	92.5
LAGO	246444	37.10	-8.67	10.0	0	12.2	-93.4	83.2
MAC1	259706	-54.50	158.94	14.2	3	8.7	-69.5	82.8
MALL	275501	39.55	2.62	12.5	-2.7	12.1	-73	85.1
MAS1	273321	27.76	-15.63	155.6	-2.9	14	-89.4	65.1
MORP	201654	55.21	-1.69	94.7	-4.8	10.2	-78.4	57.6
NEWL	167410	50.10	-5.54	11.2	-1.3	10.4	-78.4	66
OHI3	208002	-63.32	-57.90	9.6	-2.5	7.6	-48.9	47.6
ONSA	277161	57.40	11.93	9.2	1.6	9.1	-89.5	87.7
PDEL	261219	37.75	-25.66	54.8	-6.5	13.4	-98.3	90.2
PIMO	232261	14.64	121.08	52.2	-7	21.9	-133.4	121.4
QAQ1	255096	60.72	-46.05	73.4	-1.5	7.2	-64.8	75.8
RABT	265072	34.00	-6.85	44.9	1	13.6	-78.5	90.7

REYK	264495	64.14	-21.96	26.7	-1.2	7.3	-68.2	69.8
SEY1	176869	-4.67	55.48	579.3	-22.3	25.5	-147	87.7
SFER	264498	36.46	-6.21	39.7	0	12.3	-79.4	98.8
SIO3	260778	32.86	-117.25	70.1	3	13.7	-89.1	93.6
STJO	270584	47.60	-52.68	143.2	1.4	12.7	-118.5	135.5
TOW2	274411	-19.27	147.06	29.5	-7.9	17	-134.2	87.7
TROM	252343	69.66	18.94	101.0	1.3	7.1	-56.6	71.7
TWTF	264284	24.95	121.16	184.2	-2.2	19.9	-105.4	129.6
VACS	59050	-20.30	57.50	427.7	-6.1	20.4	-114.6	94.3
VALE	235101	39.48	-0.34	27.1	-2.4	13.3	-93	74.4
TOTAL	11249648				-2.3	13.1	-174.0	140.8

Tab.2 – Statistics (mean, standard deviation, minimum and maximum) of the differences between GNSS-derived and ECMWF-derived ZWD for the 127 coastal GNSS stations of Dataset2, for the period 2002-2009.

SITE NAME	NPOINTS	LAT (º)	LON (º)	HORT (m)	MEAN (mm)	SIGMA (mm)	MIN (mm)	MAX (mm)
AIRA	369137	31.82	130.60	282.9	-12.3	17.1	-128.9	84.9
ALRT	631547	82.49	-62.34	58.7	0.9	4.9	-32.5	37.1
AUT1	40434	40.57	23.00	108.3	-0.9	12.9	-74.2	64.7
BAIE	684822	49.19	-68.26	53.5	-0.7	11.2	-95	83.6
BARH	744117	44.40	-68.22	32.5	-1.3	12.6	-82.9	91.6
BDOS	254708	13.09	-59.61	10.1	2.1	15	-93.7	90.5
BELF	25177	54.58	-5.93	26.2	-0.7	9.6	-66.2	74.8
BHR2	114618	26.21	50.61	13.9	7.5	11.7	-54.6	57.7
BORR	18979	39.91	-0.08	21.9	-2.5	11.9	-61.4	84.1
BRFT	351690	-3.88	-38.43	30.4	-4	16.3	-86	120.1
BUDP	59138	55.74	12.50	58.1	-6.1	10.6	-83.9	55.3
CAGZ	417715	39.14	8.97	191.6	-2.4	13.6	-85.9	63.5
CAS1	768599	-66.28	110.52	38.8	-8.1	5	-31.2	24.1
CCJM	361369	27.10	142.18	160.8	-9.2	16.5	-107.6	88.4
CHUR	845749	58.76	-94.09	29.6	0.6	8.3	-59.7	93.6
CIC1	715058	31.87	-116.67	99.5	1.3	15.7	-83.5	149.2
CNMR	330243	15.23	145.74	11.5	-13.4	18	-115.2	104.4
COST	32654	44.16	28.66	12.6	-2.5	11.5	-72.9	65.6
CRAO	674272	44.41	33.99	363.5	-14.4	17.3	-132.9	94.4
DAKA	122518	14.69	-17.46	33.0	-11.7	15.1	-88.6	56.4
DAV1	747800	-68.58	77.97	27.0	-10.1	5	-33.5	17.6
DELF	73141	51.99	4.39	31.1	-4.6	11.6	-86.6	72.8
DLFT	705435	51.99	4.39	31.0	-0.5	10.6	-74.9	67.9
DUBR	42542	42.65	18.11	413.5	-12.4	19.5	-191.7	141.6
EPRT	709506	44.91	-66.99	54.8	-0.9	12.3	-75.7	84.7
ESCU	440904	47.07	-64.80	4.5	1.3	11.2	-80.3	76.1
EVPA	31034	45.22	33.16	14.4	-1.3	11.3	-88.6	61.1
FALE	290857	-13.83	-172.00	14.4	-7.3	19.9	-102.2	108.6
GENO	689061	44.42	8.92	111.0	-3.9	16.6	-98.5	117.3

GMAS	720946	27.76	-15.47	154.0	-3.2	13.9	-85.3	75.2
GMSD	419691	30.56	131.02	114.5	-5.9	17.4	-127.2	89.1
GUIP	36550	48.44	-4.41	103.5	-1.9	12.2	-93	57.4
GUUG	378203	13.43	144.80	80.6	-14.6	18.2	-149	70.7
HARV	501508	34.47	-120.68	52.1	2.8	11.6	-95.8	76
HERS	626304	50.87	0.34	31.7	-2.3	10.5	-73.7	75.5
HERT	479852	50.87	0.33	38.5	-2.9	10.6	-66.8	72.1
HILO	592269	19.72	-155.05	11.1	3.6	18.2	-81.4	97.3
HNLC	727640	21.30	-157.86	6.9	-5.6	17.9	-130	77.7
HNPT	712724	38.59	-76.13	8.8	-2.5	14.7	-111.8	106
HOE2	37865	54.76	8.29	22.7	-3.3	11	-93.1	67.4
HOLB	765123	50.64	-128.14	576.3	-4.4	16.4	-87.8	91.1
HOLM	781391	70.74	-117.76	56.3	-10.3	7.7	-63.2	62.6
HOLP	780297	33.92	-118.17	28.6	-3.6	15.9	-129.4	80
INVE	42507	57.49	-4.22	12.9	-7.7	11.6	-73.3	56.4
IQQE	220070	-20.27	-70.13	7.5	3.6	20.7	-69.4	124.6
KELY	355704	66.99	-50.94	198.5	0.7	7.4	-44.4	100.8
KOUC	475374	-20.56	164.29	24.2	-5.5	17.3	-117.8	114.3
KSMV	660052	35.96	140.66	23.5	-6.5	15.1	-118.5	83.2
KUUJ	553131	55.28	-77.75	42.7	-1	10.2	-83.4	83.7
LAE1	335870	-6.67	146.99	69.3	-0.3	30.1	-137.1	133.8
LAMP	61804	35.50	12.61	20.1	-9	15	-120	76.8
LBCH	717430	33.79	-118.20	8.5	-2.8	15.4	-144.1	84.8
LPGS	561881	-34.91	-57.93	14.2	-3.4	16.7	-110.1	106.3
LROC	343923	46.16	-1.22	10.0	-3.7	11.9	-70.9	66.3
MAG0	494754	59.58	150.77	344.9	2.3	10	-91	78.1
MALD	224958	4.19	73.53	5.7	4.5	17.5	-77.9	73.9
MAR-06	678130	60.60	17.26	50.8	-2.4	9.7	-64.2	59
MAW1	648969	-67.60	62.87	30.1	-4.9	4.4	-27.8	17.8
MCIL	222588	24.29	153.98	11.5	-8.7	13.6	-75.1	51.4
MCM4	662624	-77.84	166.67	151.6	-5.6	6.3	-33.5	23.1
METS	689205	60.22	24.40	76.0	-1	9	-61.5	72.4
METZ	652561	60.22	24.40	75.9	-0.8	9.2	-55.3	69.7
MIKL	537215	46.97	31.97	68.7	1.1	12.1	-96	92.5
MOBS	518507	-37.83	144.98	35.6	0.9	10.9	-119.7	77.6
MTKA	677189	35.68	139.56	71.9	-4.3	14.9	-96	94.1
NANO	848165	49.29	-124.09	24.0	-0.4	12	-87.1	83.8
NKLG	801401	0.35	9.67	21.6	-7.8	23.6	-107.3	99
NOA1	30939	38.05	23.86	498.9	-4.2	16.6	-104	65.1
NOT1	660698	36.88	14.99	85.5	-2.5	15.8	-87.7	84.7
NTUS	616223	1.35	103.68	72.1	-20.7	17.5	-104.1	59.2
NYA1	708067	78.93	11.87	47.7	-0.4	5.8	-51.9	38.8
OHI2	695236	-63.32	-57.90	10.1	-5	7.1	-37.2	29.8
OSLS	72047	59.74	10.37	181.7	-4.9	10.6	-71.4	58.7
OSN1	70634	37.08	127.02	25.8	0.6	9.4	-47.5	49.6
OSN2	61483	37.08	127.02	25.8	0.8	8.8	-48.3	49.6

OUS2	654686	-45.87	170.51	21.1	-1.6	11.4	-87.6	73
PADO	355644	45.41	11.90	20.3	-2.4	12.3	-67.1	78.9
PARC	393055	-53.14	-70.88	13.4	0.1	9.5	-48.9	74.5
PERT	778694	-31.80	115.89	45.6	0.9	11.5	-80.7	79
PETP	663113	53.07	158.61	188.7	-0.4	9.1	-122.2	70.1
PETS	485159	53.02	158.65	80.2	-6.6	8.5	-70.4	61.2
QIKI	529523	67.56	-64.03	6.7	-1.5	7.1	-69.4	59.6
RBAY	365225	-28.80	32.08	7.8	-6.6	17.3	-101.7	77.6
RESO	748773	74.69	-94.89	43.5	-3.4	5.9	-38.5	52.3
RIGA	567109	56.95	24.06	14.3	-1.6	10	-73.6	73.4
ROAP	139189	36.46	-6.21	29.2	-6.8	11.2	-53.5	47
SASS	122732	54.51	13.64	32.9	-0.7	9.6	-59	52.3
SCIP	695774	32.91	-118.49	490.7	3.4	19.2	-125.7	78.5
SCOR	390674	70.49	-21.95	72.8	-0.3	5.8	-34.6	34.5
SCUB	581181	20.01	-75.76	47.4	-3.6	22.1	-126	112.5
SHE2	195115	46.22	-64.55	4.8	3.2	11	-62	103.6
SIMO	345209	-34.19	18.44	8.7	-3.9	11.9	-84.9	68.9
SKE0	52875	64.88	21.05	59.2	-3.7	9.1	-59.8	67.2
SLOR	106335	13.42	-87.44	8.6	-6.3	24	-95.5	90.3
SMID	55319	55.64	9.56	82.7	-6.4	11.3	-89.3	64.7
SNI1	852966	33.25	-119.52	277.4	3.1	15.2	-97	97.9
SPK1	832810	34.06	-118.65	476.5	1.1	17.8	-142.5	115.6
STAS	71608	59.02	5.60	61.0	-8	10.7	-79.3	54.7
SUUR	25159	59.46	24.38	65.9	1.3	9.2	-57.3	62.7
SUWN	787332	37.28	127.05	60.9	-7.5	13.3	-105	71.6
SYDN	363687	-33.78	151.15	62.9	-4.5	12.3	-85.4	71
SYOG	815544	-69.01	39.58	28.2	-3	4.7	-32	24
TCMS	687692	24.80	120.99	58.4	7.5	21.8	-92.6	146.5
TERS	72792	53.36	5.22	14.9	-4.7	11.4	-88.9	65.7
TGCV	51436	16.75	-22.98	6.5	-4.7	12.5	-55.6	59.2
THTI	802355	-17.58	-149.61	91.9	-3.5	18.4	-94.6	84.8
THU2	675254	76.54	-68.83	19.5	-1.5	6.1	-40.2	46.6
THU3	575983	76.54	-68.83	19.4	-2.3	5.9	-38.5	47.9
TIXI	791350	71.63	128.87	53.9	0	7.7	-54.5	111.8
TNML	639711	24.80	120.99	57.0	8	21.9	-90.3	148.2
TORP	794599	33.80	-118.33	31.3	-1.4	15.4	-145.7	86.9
TRAB	535919	40.99	39.78	74.8	5.7	23.5	-105.4	163.3
TRAK	826258	33.62	-117.80	151.9	-2.2	19.1	-126.3	80.8
TRDS	70402	63.37	10.32	277.7	-5.9	10.4	-76	57
TRO1	720947	69.66	18.94	107.1	-0.4	7.6	-55.4	64.2
TUBI	724036	40.79	29.45	183.0	-8.9	12.9	-105.9	49
TUC2	43277	35.53	24.07	137.5	-1.1	13.5	-78.6	73.1
TUKT	631501	69.44	-132.99	8.5	1.2	7.6	-46.2	61.2
UCLP	866478	34.07	-118.44	147.1	-1.6	16.3	-131.6	106.4
UCLU	897277	48.93	-125.54	29.3	-1.9	10.9	-84.4	72.6
USC1	860836	34.02	-118.29	57.2	-0.3	17.2	-123.4	91.2

VAAS	71125	62.96	21.77	40.2	-7	10.5	-76	113.7
VALP	153849	-33.03	-71.63	10.2	-0.2	14.8	-98.6	48.4
VARS	70818	70.34	31.03	156.9	-4.1	9.8	-80.5	56.8
VIS0	669431	57.65	18.37	55.0	-1.5	9.5	-66	68.8
VNDP	757169	34.56	-120.62	25.3	1.4	13.2	-94.2	79.1
WARN	121022	54.17	12.10	12.7	-1.4	9.3	-62.4	49.9
TOTAL	58838533				-2.9	12.9	-191.7	163.3

Tab.3 – Statistics (mean, standard deviation, minimum and maximum) of the differences between GNSS-derived and ECMWF-derived ZWD for the 17 coastal GNSS stations of Dataset 3, for the period 2002-2009.

SITE NAME	NPOINTS	LAT (º)	LON (º)	HORT (m)	MEAN (mm)	SIGMA (mm)	MIN (mm)	MAX (mm)
AJAC	120174	41.93	8.76	49.4	2.6	15	-71.5	121.3
ALAC	162580	38.34	-0.48	10.1	-0.5	13.6	-102.7	81.1
ALME	190638	36.85	-2.46	77.3	6.6	16.5	-101.5	112.1
BRST	145347	48.38	-4.50	14.5	-1.4	11	-93.8	67.7
CANT	201477	43.47	-3.80	49.4	0.5	11.6	-65.4	77.6
CEU1	157644	35.89	-5.31	10.7	-1	14	-73.6	92.5
CREU	193514	42.32	3.32	84.0	-6.1	14.6	-94.6	83.6
EBRE	196852	40.82	0.49	57.8	-0.8	14.9	-80.1	87
ELBA	200950	42.75	10.21	223.6	-2.6	14.8	-106.4	91.7
GOUG	110733	-40.35	-9.87	58.1	-0.3	13.9	-98.7	99.9
HUEL	11090	37.20	-6.92	30.3	0.5	10.8	-48.9	66.5
KOUR	193362	5.25	-52.81	8.8	-0.8	17.4	-115.9	107.2
MALA	76600	36.73	-4.39	72.1	3.5	13.4	-101.4	69.8
MARS	173630	43.28	5.35	12.6	3.7	12.6	-80.8	97.4
MILO	96352	38.01	12.58	49.2	-1.6	11.1	-67.4	59.4
NAIN	171426	56.54	-61.69	43.4	3.6	8.7	-76.4	77.7
VIGO	68817	42.18	-8.81	32.1	-0.8	11	-61.3	66.9
TOTAL	2471186				0.3	13.2	-115.9	121.3

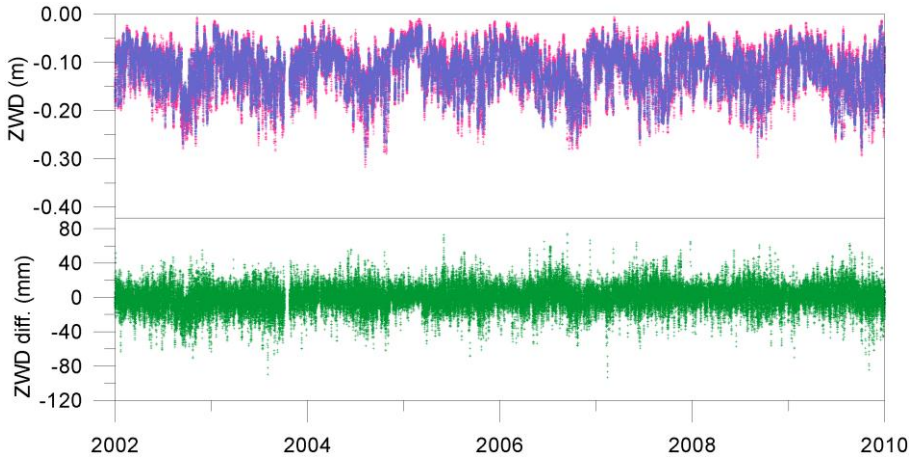

Fig.7 – Comparison between GNSS and ECMWF-derived ZWD for station CASC. red – ZWD from GNSS (m); blue – ZWD from ECMWF (m); green – difference between GNSS and ECMWF-derived ZWD (mm).

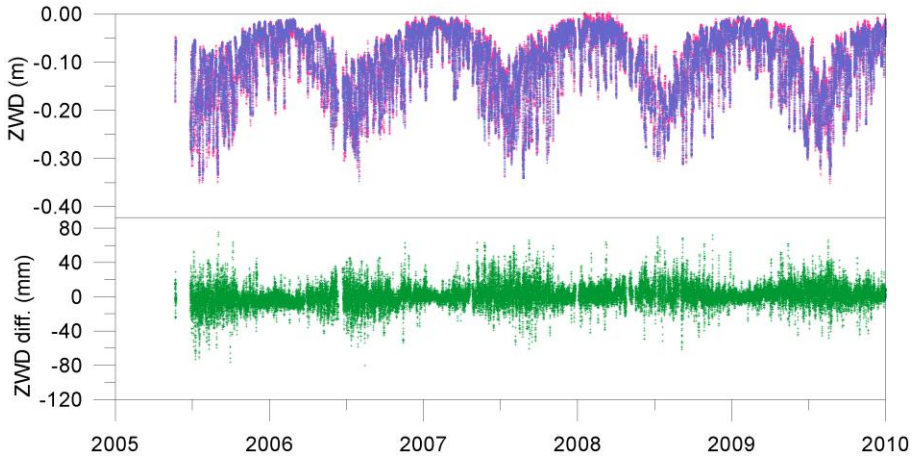

Fig.8 – Comparison between GNSS and ECMWF-derived ZWD for station ESCU. red – ZWD from GNSS (m); blue – ZWD from ECMWF (m); green – difference between GNSS and ECMWF-derived ZWD (mm).

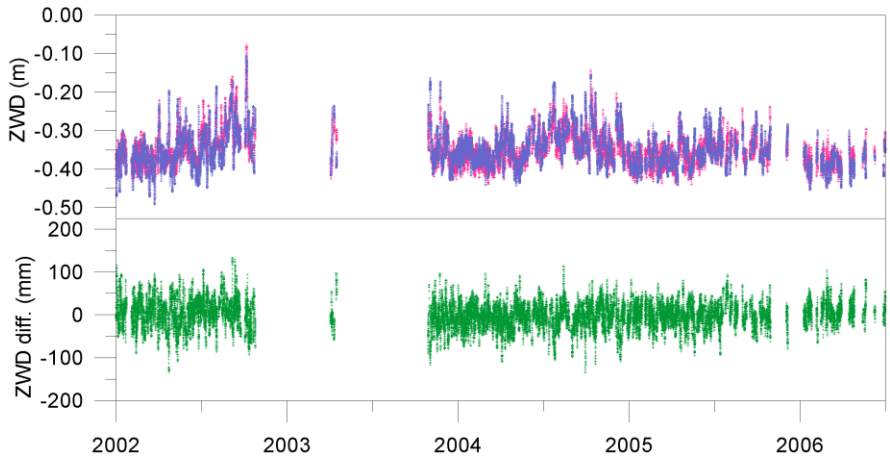

Fig.9 – Comparison between GNSS and ECMWF-derived ZWD for station LAE1. red – ZWD from GNSS (m); blue – ZWD from ECMWF (m); green – difference between GNSS and ECMWF-derived ZWD (mm).

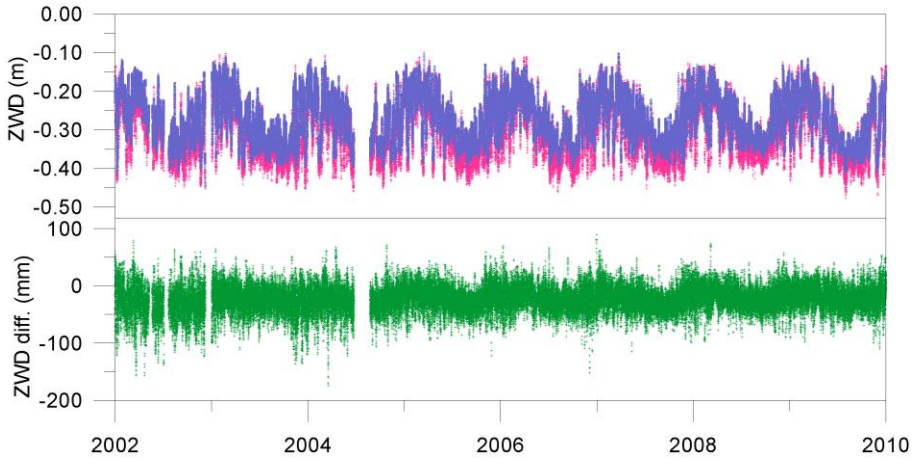

Fig.10 – Comparison between GNSS and ECMWF-derived ZWD for station GUAM. red – ZWD from GNSS (m); blue – ZWD from ECMWF (m); green – difference between GNSS and ECMWF-derived ZWD (mm).

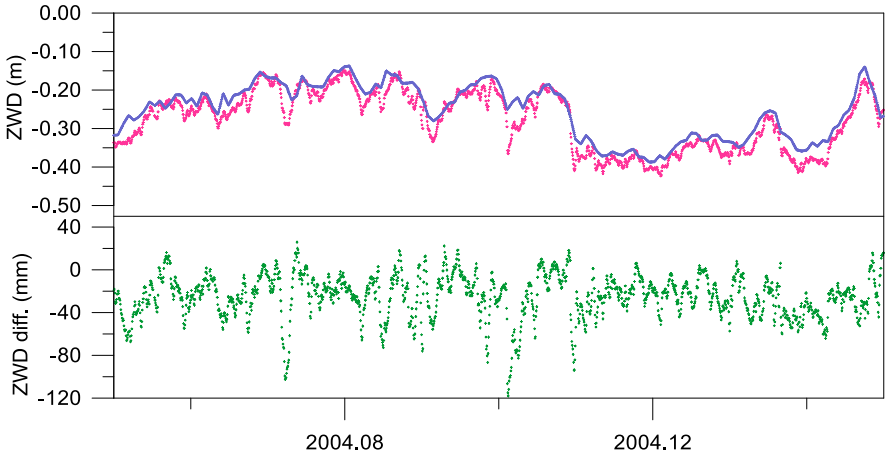

Fig.11 – Comparison between GNSS and ECMWF-derived ZWD for station GUAM for a small period. red – ZWD from GNSS (m); blue – ZWD from ECMWF (m); green – difference between GNSS and ECMWF-derived ZWD (mm).

2.3 Comparison between GNSS-derived and MWR-derived ZWD

For use in this study, Envisat MWR data have been stacked. For each measurement point at each epoch of an Envisat cycle, the MWR correction and associated flags are interpolated to the positions along the reference tracks, using spline interpolation. Then for each satellite measurement point, the ZWD from the closest GNSS station is interpolated for the associated measurement epoch. This methodology is slightly different from the one adopted in [RD2], where the comparison was made for all stations in the vicinity of each satellite measurement. The experience acquired since then and the large amount of data to be analysed indicated that the comparison with the closest station is the most efficient and recommended procedure. In addition, the comparison is only made for points within a specified distance of the closest station.

The algorithm to perform this analysis was implemented in Fortran90. It performs the analysis for any satellite, number of cycles and stations. The limit

is imposed by the maximum of allocatable memory. In the present study the algorithm was run for 190 stations, 76 Envisat cycles (cycles 10 to 85), covering the period 2002-2009.

To reduce the amount of data to be processed, only satellite data within a distance of 300 km from the coast were selected. Figure 12 represents the selected data for Envisat cycle 58. As explained in section 1, data were obtained from RADS by extracting all ocean altimeter measurements without applying any rejection criteria. For Envisat, the MWR wet tropospheric correction (ZWD_MWR) is considered to have valid values if the radiometer land/ocean flag (MWR_LO) is 0, the MWR quality interpolation flag (MWR_QUAL) is 0 and $0 < \text{ZWD\_MWR} \leq 0.5$ m. Only valid measurements are used in the study presented in this section. Considering this coastal dataset, the stacked data have 1002 passes and a maximum number of 1470 points per pass. The maximum number of points per station is 277 200 (one point every 15 seconds or larger).

On a first run, for a given GNSS station dataset and for each point along the reference tracks, the program identifies the closest station and computes its distance from the satellite reference ground track point. On the second run, for each point along the passes of a given cycle, it interpolates the ZWD from the closest station, for the measurement's epoch.

The program computes and stores the ZWD for all points along the satellite reference tracks and all epochs of each cycle. Three different ZWD values are stored: from the MWR (ZWD_MWR), from ECMWF (ZWD_MOD) and interpolated from the closest GNSS station (ZWD_GNSS). The values ZWD_MOD are those present on the RADS data base, which have been extracted from the Geophysical data Records (GDR).

Data can be grouped, for example, by station, cycle, pass or region, allowing multiple analyses. The time series of the mentioned wet tropospheric delays are inter-compared by computing various statistics: correlation, mean, standard deviation, minimum and maximum.

The first comparison showed large differences in a number of points and stations. The results of the previous section indicated that these differences could not be attributed to the GNSS data. A close inspection revealed that the MWR data can be quite noisy at high latitudes and that these noisy data can have decimetre differences with respect to the closest GNSS station. It was also found that these noisy MWR values were mostly associated to the value 1 in the radiometer ice flag (MWR_ice). It was then decided to perform the analysis only with data with MWR_ice = 0. Figure 13 illustrates the measurements with MWR_ice = 1 for Envisat cycle 58. For this cycle, 21% of the coastal measurements represented in this figure have an ice flag set to 1. It can be observed that this criterion removes most of the valid measurements north of 60° and south of -60°, preventing an appropriate analysis for some stations located at high latitudes.

In the subsequent analysis, by "all measurements" we mean all points along the satellite reference tracks at the 76 different epochs of Envisat cycles 10 to 85. By "track points" we mean locations on the satellite reference ground tracks. For each track point there can be up to 76 measurements, one for each Envisat cycle.

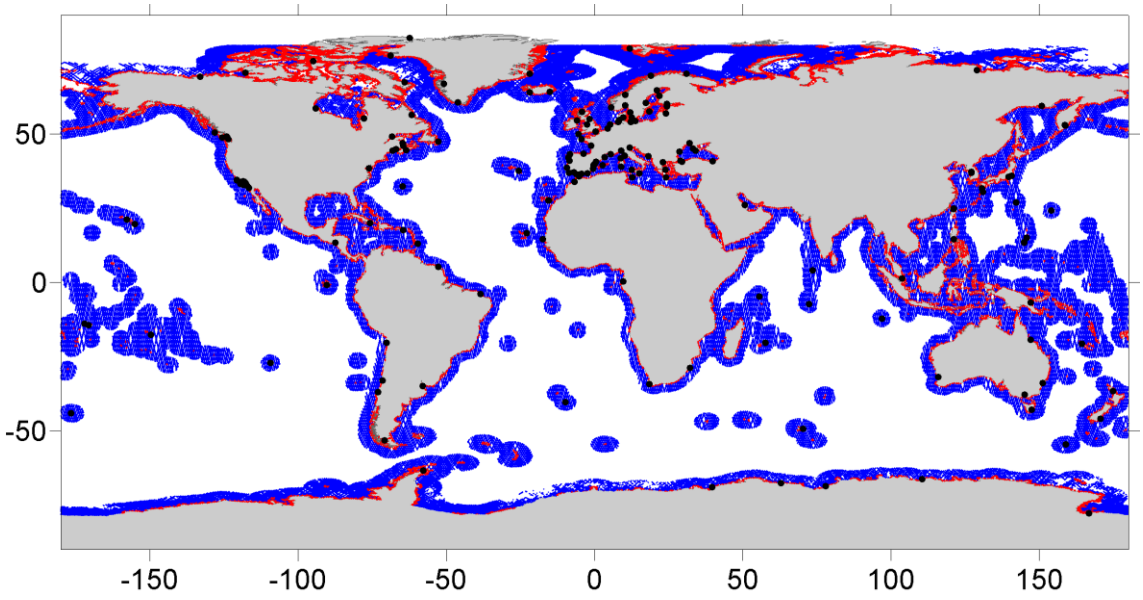

Fig.12 – Location of Envisat coastal data (points up to 300 km from land) for cycle 58. blue – points with valid MWR wet tropospheric correction (MWR_LO flag =0 and MWR_QUAL flag =0); red – points with invalid wet tropospheric correction (MWR_LO flag ≠0 or MWR_QUAL flag ≠0 or Wet_MWR out of limits). Black circles: location of the set of 190 coastal stations with available ZWD solutions field.

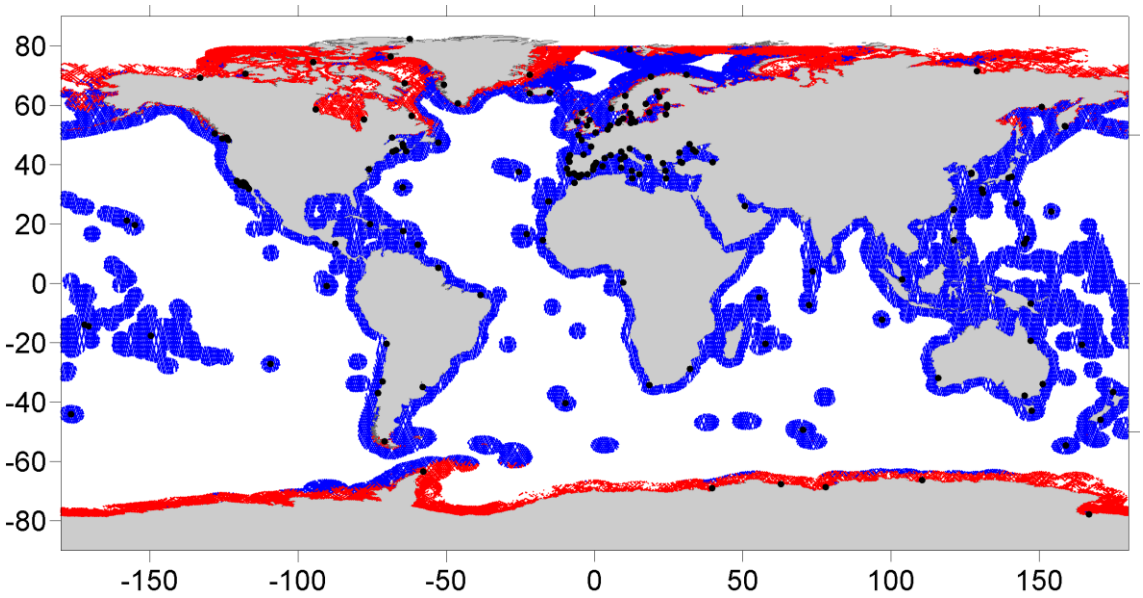

Fig.13 – Location of Envisat coastal data (points up to 300 km from land) for cycle 58. blue – points with MWR_ice flag =0; red – points with MWR_ice flag =1. Black circles: location of the set of 190 coastal stations with available ZWD field.

The analysis will focus mainly on the statistics of the differences for all measurements, for each of the 190 stations. Unless different values are specified, the comparisons were performed for satellite track points located at distances $\geq$ 20 km from the coast and $\leq$ 100 km from the closest station.

A number of 46 stations do not have enough data for the analysis. We consider in this group all stations with a total number of measurements less than 76. These are shown in Figure 14. Some of these stations are located in regions where the MWR measurements were rejected due to the radiometer ice flag. However, there are stations which were excluded from this analysis because they are never the closest station to any satellite point due to its location and to the fact that there is another station in its vicinity closest to the same track points. This prevents the analysis of some stations which can be analysed separately in a future study. However, from the point of view of comparing each point on the satellite track with the closest GNSS station, the adopted approach is the correct one.

From the remaining stations, 7 possess a correlation < 0.7 (CAS1, DAV1, ESCU, MCM4, MAW1, SYOG) or a standard deviation > 30 mm (station STJO) and are analysed separately.

For the group of 136 stations which were considered to have enough data for the comparison, the statistics of the differences between GNSS and MWR ZWD is: 0.93, -5.8, 20.0, -430.0, 224.9 mm for the correlation, mean, standard deviation, minimum and maximum respectively. The detailed results for each station are presented in table 4. Figure 16 represents a time series of the points for a typical station (CASC) within this group.

A detailed inspection of the set of 7 stations with a very small correlation or very large sigma is required. Here we present the first results of this analysis. So far, it can be observed that none of these stations reveal any problem in the comparison with ECMWF shown in section 2.1. To facilitate the analysis, these stations have been highlighted in grey in tables 1 and 2. It can be observed that these stations are very stable when compared with ECMWF.

Therefore, it appears that the strange results for these stations might be caused by noisy MWR measurements.

Figures 17 and 18 represent the ZWD time series for all points in the vicinity of stations ESCU and STJO. These are the only two stations which possess a very low correlation or very large sigma and are not at extreme latitudes. Figures 20 and 21 show the similar time series for stations CAS1 and SYOG, located near the Antarctica. In all cases, it is evident that the MWR measurements can be very noisy. In the last case this shall be due to ice contamination; in the first case it can be due to land or ice contamination in the radiometer.

-

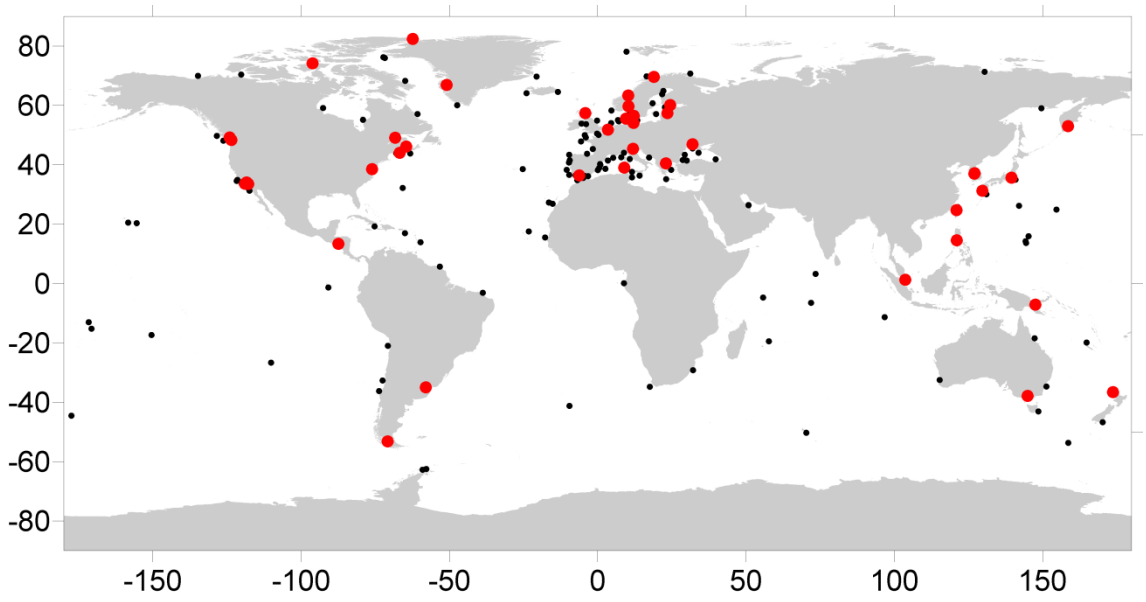

Fig.14 – black: set of 136 stations with available data for the comparison. red – 47 stations for which the number of available satellite points for the comparison is < 76.

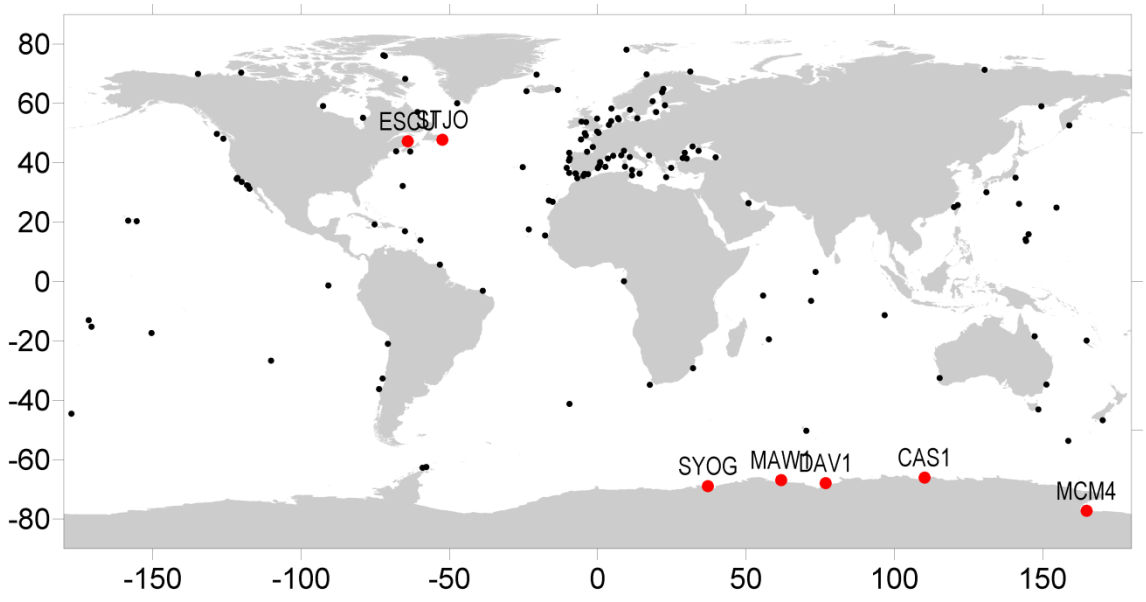

Fig.15 – – black: set of 136 stations with available data for the comparison. red – stations for which the correlation between GNSS and MWR ZWD is < 0.7 (6 stations: CAS1, DAV1, ESCU, MCM4, MAW1, SYOG) or the standard deviation of the differences is > 40 mm (STJO).

Tab.4 – Statistics (correlation, mean, standard deviation, minimum and maximum) of the differences between GNSS-derived and MWR-derived ZWD for the 137 coastal GNSS stations for which there are enough satellite points for the comparison.

NAME	NP	LON	LAT	COR	MEAN	SIGMA	MIN	MAX
ACOR	2717	-9.61	43.39	0.89	-2.6	21.1	-132.9	160.1
AJAC	1378	7.93	42.57	0.91	-8.8	18.9	-72.5	68.4
ALAC	1492	0.02	38.25	0.94	-0.8	17.6	-44.9	70.7
ALME	2982	-3.24	36.21	0.90	1.1	20.9	-105.5	90.0
ASPA	5388	-170.67	-15.20	0.91	-1.4	25.7	-128.3	155.3
BARH	1608	-68.00	43.91	0.96	-8.2	20.2	-69.8	125.7
BDOS	2481	-59.74	13.95	0.91	-3.8	24.2	-70.5	156.3
BELF	102	-5.46	53.94	0.95	2.9	17.6	-38.0	48.0
BHR1	925	50.82	26.42	0.91	6.8	18.6	-48.3	110.0
BHR2	203	50.83	26.48	0.94	8.0	18.3	-36.3	66.5
BORR	552	0.87	40.07	0.91	-0.9	23.1	-54.6	95.3
BRFT	1267	-38.72	-3.06	0.94	-2.4	21.4	-49.3	141.8
BRMU	7654	-65.74	32.23	0.95	-7.2	23.1	-125.7	193.1
BRST	1021	-5.63	47.91	0.91	-5.2	19.6	-89.4	206.1
CAGZ	2388	9.21	38.72	0.94	-5.7	16.4	-63.8	63.7
CANT	3346	-3.63	43.76	0.94	-7.6	16.2	-69.4	58.9
CASC	3788	-10.47	38.37	0.93	-0.3	17.4	-79.6	83.0
CCJM	3318	142.03	26.26	0.96	-4.9	25.4	-113.3	184.4
CEU1	862	-4.85	35.61	0.94	-0.2	14.3	-45.1	50.5
CHAT	6276	-177.44	-44.53	0.93	-3.1	16.2	-81.8	178.9
CHUR	1223	-92.58	59.19	0.95	-13.7	15.7	-63.5	109.9
CIC1	1884	-117.46	31.33	0.95	-7.1	16.0	-75.8	29.5
CNMR	2576	145.30	15.98	0.95	4.0	21.5	-78.6	148.4
COCO	6993	96.78	-11.33	0.95	-0.1	20.8	-133.1	147.9
CONZ	1281	-73.69	-36.16	0.93	-4.8	14.0	-68.6	41.0
COST	1539	29.31	43.43	0.94	-10.6	18.1	-76.3	129.8
CRAO	2816	33.98	44.06	0.95	-24.3	21.0	-96.8	46.0
CREU	5181	3.46	41.44	0.94	-8.5	18.5	-97.4	67.9
CRO1	3894	-65.02	17.00	0.93	-2.1	20.6	-119.4	134.6
DAKA	817	-17.71	15.52	0.98	-3.3	17.4	-64.4	62.2
DARE	365	-3.93	53.74	0.95	-4.7	14.6	-59.2	45.6
DELF	2253	3.74	52.79	0.94	-7.0	17.7	-83.1	65.4
DGAR	5363	71.98	-6.48	0.91	-1.9	24.1	-96.3	172.7
DUBR	1190	17.30	42.47	0.92	-22.4	22.2	-89.1	70.1
EBRE	675	0.79	40.30	0.92	-2.2	22.6	-57.1	83.6
ELBA	634	10.84	41.99	0.93	-9.9	18.1	-59.7	62.9
EVPA	1278	32.01	45.51	0.95	-9.7	16.7	-60.9	42.2
FALE	933	-171.58	-13.03	0.93	7.4	26.6	-65.6	127.3
GAIA	2264	-9.69	40.79	0.92	-7.8	19.7	-109.7	55.8
GENO	1459	8.82	44.10	0.94	-10.2	21.6	-80.8	80.9
GLPS	1484	-90.85	-1.26	0.95	-12.6	13.0	-63.0	49.7
GMAS	4163	-15.17	26.91	0.91	0.9	19.2	-92.0	62.1

GMSD	2240	131.02	30.09	0.97	-0.8	30.6	-430.0	111.9
GOUG	3470	-9.55	-41.19	0.94	-3.5	17.6	-93.4	96.1
GUAM	2776	144.26	14.25	0.93	-8.8	25.2	-130.3	112.5
GUIP	1242	-3.99	49.25	0.92	-5.4	18.4	-93.1	50.7
GUUG	1705	144.40	13.67	0.95	0.7	22.5	-136.4	121.9
HARV	2065	-121.76	34.62	0.90	-5.2	17.8	-78.6	93.4
HELG	3251	7.10	54.66	0.96	-4.4	13.0	-59.6	43.6
HERS	735	0.31	50.07	0.96	-1.3	12.7	-59.6	52.8
HERT	848	-0.23	50.50	0.95	-2.0	14.1	-73.4	44.9
HILO	3002	-155.47	20.41	0.88	-8.3	21.3	-80.7	193.8
HLFX	2025	-63.23	43.86	0.95	-5.2	23.7	-167.9	215.1
HNLC	3876	-158.31	20.55	0.91	3.7	18.6	-61.9	139.8
HOB2	854	148.60	-43.08	0.92	1.9	15.8	-53.2	76.5
HOE2	1896	6.86	55.11	0.95	-6.3	15.1	-61.6	52.4
HOFN	6000	-13.44	64.58	0.93	-0.6	14.2	-47.9	68.0
HOLB	2730	-128.42	49.81	0.92	-15.6	20.9	-100.7	45.1
HOLM	1888	-120.19	70.40	0.90	-20.1	15.3	-53.1	93.8
HUEL	357	-7.48	36.44	0.92	1.4	18.3	-47.8	135.4
IQQE	637	-70.72	-20.98	0.96	-16.2	13.3	-71.4	14.4
ISPA	6053	-110.11	-26.59	0.94	-3.7	18.4	-145.6	135.0
ISTA	1391	28.69	41.65	0.95	-14.6	16.2	-68.7	75.3
KERG	4870	70.33	-50.21	0.94	-1.6	11.8	-73.0	70.3
KOUC	2016	164.87	-19.88	0.96	3.9	22.1	-68.1	111.2
KOUR	2548	-53.19	5.76	0.89	-13.7	21.4	-82.9	189.5
KSMV	2314	140.86	35.07	0.97	-9.6	26.9	-103.9	224.9
KUUJ	467	-79.10	55.20	0.95	-11.2	16.0	-58.0	93.5
LAGO	4214	-9.58	36.61	0.92	-1.9	16.7	-66.1	152.1
LAMP	7458	11.56	35.76	0.92	-15.8	18.6	-81.6	168.4
LROC	1261	-1.61	45.33	0.96	-4.3	13.9	-54.3	67.4
MAC1	12037	158.63	-53.63	0.93	-3.4	11.5	-71.8	75.3
MAG0	150	149.64	59.09	0.96	-10.7	16.3	-58.8	35.1
MALA	835	-4.40	36.27	0.94	0.0	15.4	-53.1	47.0
MALD	974	73.45	3.32	0.93	-7.0	19.4	-74.4	105.9
MALL	4276	2.56	38.68	0.94	-4.5	16.2	-90.6	89.4
MAR6	1522	18.53	60.80	0.96	-9.9	12.8	-68.9	65.4
MARS	1488	5.24	42.43	0.95	2.2	17.2	-69.0	73.6
MAS1	2180	-16.50	27.30	0.96	1.5	14.6	-56.0	51.4
MCIL	2608	154.64	24.93	0.96	0.7	20.6	-96.4	186.1
MILO	3135	11.57	37.63	0.91	-6.4	17.7	-72.0	78.8
MORP	2624	-0.21	54.91	0.94	-8.3	15.0	-54.5	100.5
NAIN	671	-60.76	57.13	0.95	-3.2	16.4	-87.3	82.2
NEWL	4429	-4.34	50.05	0.93	-3.9	16.4	-88.7	140.4
NKLG	864	8.81	0.16	0.80	-8.8	21.6	-45.9	158.1
NOA1	85	24.74	38.38	0.91	-15.4	19.3	-49.0	42.2
NOT1	3336	14.06	36.39	0.93	-15.3	17.7	-82.1	191.8
NYA1	9862	9.66	78.17	0.92	-6.1	11.9	-51.4	99.9
OHI2	1028	-57.82	-62.46	0.72	-2.4	14.8	-32.3	90.0
OHI3	1486	-59.04	-62.72	0.73	0.7	15.6	-40.8	97.7
ONSA	441	10.87	57.94	0.96	-2.1	12.1	-40.9	47.5

OUS2	3596	170.24	-46.70	0.93	-8.4	13.2	-60.0	70.2
PDEL	6164	-25.24	38.58	0.94	-7.1	17.6	-88.3	100.9
PERT	354	115.27	-32.50	0.87	2.9	17.4	-53.8	49.4
PETS	1019	159.02	52.64	0.97	-16.9	15.7	-71.6	17.1
QAQ1	2002	-47.35	60.10	0.93	-1.6	14.6	-45.3	90.8
QIKI	1226	-64.93	68.28	0.88	-3.4	20.4	-38.9	107.0
RABT	1851	-6.86	34.88	0.93	-8.2	18.2	-72.0	72.6
RBAY	1509	32.12	-29.17	0.93	-5.6	25.7	-67.6	184.9
REYK	3736	-24.00	64.19	0.92	-1.3	14.1	-70.9	51.3
ROAP	352	-7.29	36.32	0.91	-10.7	20.9	-67.1	200.8
SASS	794	13.36	55.04	0.97	-4.3	9.8	-33.4	28.0
SCIP	1871	-118.28	32.50	0.94	-0.5	16.8	-58.9	56.7
SCOR	917	-20.61	69.72	0.77	3.7	23.2	-49.8	102.5
SCUB	1453	-75.27	19.26	0.92	-1.0	24.9	-71.8	132.6
SEY1	2896	55.77	-4.68	0.91	-24.7	29.0	-106.5	114.3
SIMO	1533	17.62	-34.77	0.90	-3.7	17.9	-55.1	63.8
SIO3	1808	-117.90	32.32	0.94	-2.8	16.0	-86.1	36.6
SKE0	1736	22.18	64.91	0.95	-8.0	14.9	-63.1	98.9
SNI1	4201	-120.01	33.56	0.94	-1.8	16.0	-115.9	41.9
STAS	3525	4.64	58.32	0.93	-8.9	16.1	-105.5	62.9
SUUR	147	22.63	59.46	0.98	-1.4	8.9	-20.2	20.0
SYDN	891	151.30	-34.65	0.94	-2.6	16.9	-77.3	59.6
TERS	5125	4.50	54.13	0.94	-7.6	15.3	-75.0	72.6
TGCV	301	-23.22	17.59	0.99	-5.2	11.6	-38.2	17.7
THTI	5340	-150.48	-17.27	0.91	-1.0	25.0	-101.4	202.2
THU2	1325	-71.75	76.01	0.84	-6.0	14.8	-38.6	97.3
THU3	636	-72.32	76.27	0.87	-6.1	14.7	-33.3	99.1
TIXI	607	130.47	71.33	0.82	-8.7	22.2	-43.3	124.5
TNML	1449	120.10	25.13	0.96	-13.5	28.3	-139.1	169.1
TOW2	1681	147.27	-18.42	0.96	4.7	23.1	-258.8	93.6
TRAB	1343	39.78	41.89	0.96	-17.7	17.8	-93.2	72.2
TROM	2061	16.44	69.81	0.95	-7.3	12.3	-71.3	31.1
TUBI	92	30.05	41.44	0.94	-14.6	17.1	-59.8	33.6
TUC2	2378	23.06	35.23	0.89	-14.6	18.1	-80.4	86.7
TUKT	663	-134.80	70.04	0.81	-10.4	19.8	-60.6	115.4
TWTF	1484	121.36	25.80	0.96	-25.5	26.7	-128.2	82.2
UCLU	3473	-126.23	48.20	0.94	-12.0	15.3	-63.4	80.9
VAAS	1176	21.72	63.84	0.94	-11.8	15.9	-78.3	63.0
VACS	1250	57.69	-19.42	0.95	-8.9	25.5	-84.1	117.9
VALE	1062	0.47	38.90	0.95	-2.8	18.7	-52.9	71.3
VALP	396	-72.55	-32.65	0.88	-10.8	16.7	-59.8	20.8
VARS	7888	31.24	70.73	0.95	-13.6	13.8	-74.3	98.2
VIGO	1407	-9.42	41.59	0.94	-5.0	16.9	-83.5	68.5
VIS0	4096	19.73	57.14	0.95	-6.3	14.4	-73.0	85.7
VNDP	567	-121.46	34.92	0.86	-5.8	19.1	-83.5	84.2

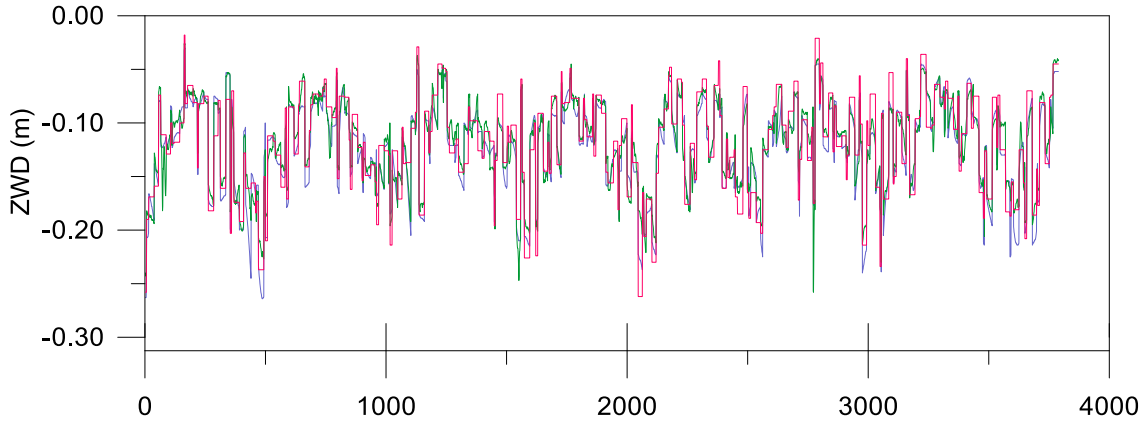

Fig.16 – ZWD time series for points in the vicinity of station CASC in metres. The x axis is point number by ascending time order. red – ZWD from GNSS; blue – ZWD from ECMWF; green – ZWD from MWR.

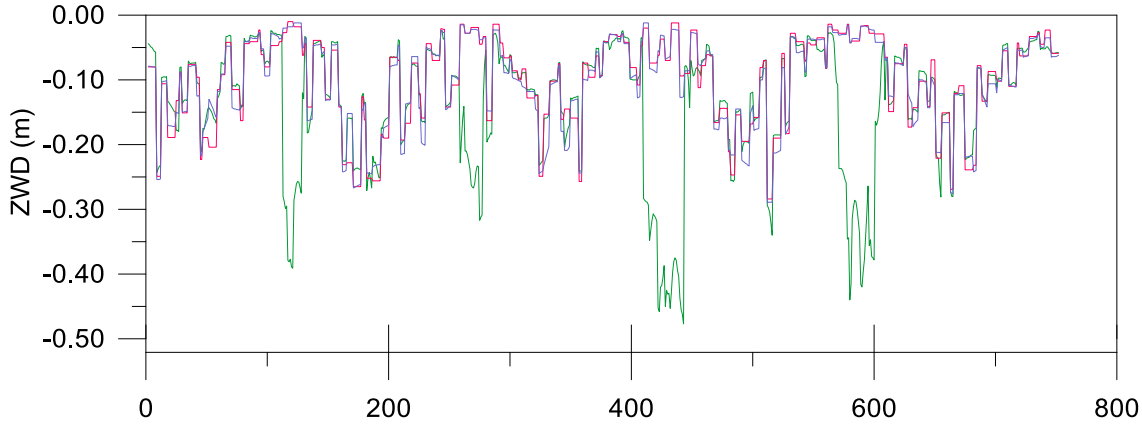

Fig.17 – ZWD time series for points in the vicinity of station ESCU in metres. The x axis is point number by ascending time order. red – ZWD from GNSS; blue – ZWD from ECMWF; green – ZWD from MWR.

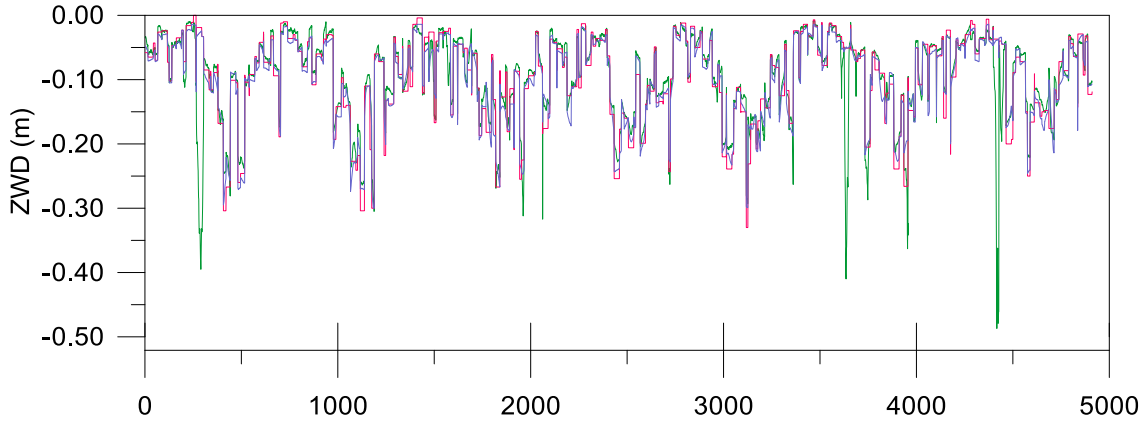

Fig.18 – ZWD time series for points in the vicinity of station STJO in metres. The x axis is point number by ascending time order. red – ZWD from GNSS; blue – ZWD from ECMWF; green – ZWD from MWR.

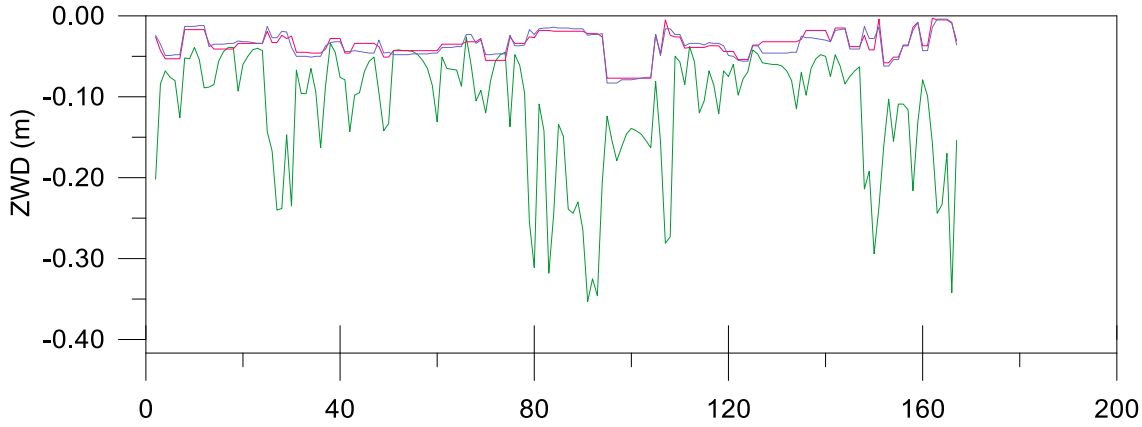

Fig.19 – ZWD time series for points in the vicinity of station SYOG in metres. The x axis is point number by ascending time order. red – ZWD from GNSS; blue – ZWD from ECMWF; green – ZWD from MWR.

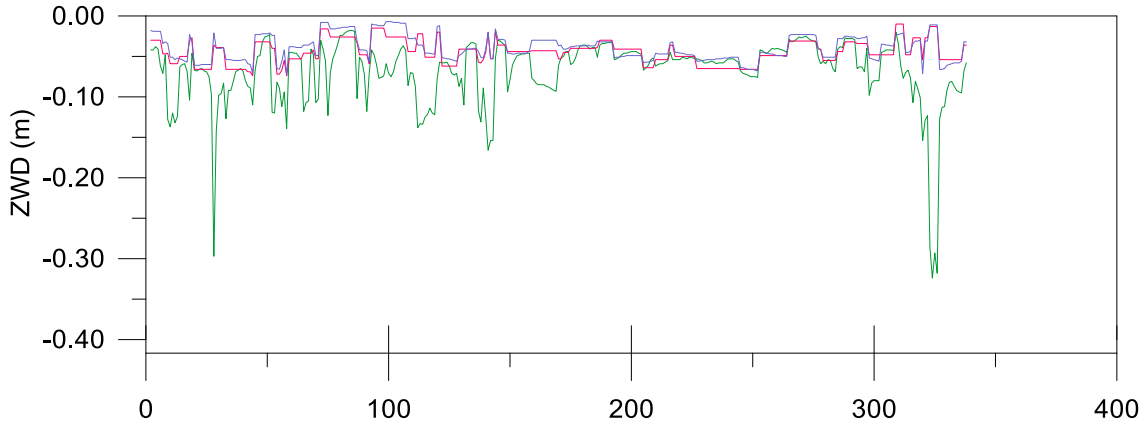

Fig.20 – ZWD time series for points in the vicinity of station CAS1 in metres. The x axis is point number by ascending time order. red – ZWD from GNSS; blue – ZWD from ECMWF; green – ZWD from MWR.

Concerning the set of stations shown in Table 4, five of them have a mean difference with an absolute value larger than 20 mm. These stations have been highlighted in blue in tables 4, 1 and 2. It can be observed that in all except TWTF there seems to be a consistent mean negative difference between the GNSS and both ECMWF and the MWR (GNSS ZWD being more negative and implying a larger path delay). However, for station TWTF the negative bias relative to the MWR is not present in the comparison with ECMWF, we can conclude that, even with such an exhaustive analysis, is very difficult to ascertain the computed mean differences to biases in the GNSS-derived path delay.

The plots shown in Figures 17 to 20, where the appearance of noisy MWR values is evident, seem to indicate that the extreme differences shown on stations presented in table 4 shall also be due to a few noisy MWR measurements, most probably due to land, rain or ice contamination.

3 GPD global implementation

3.1 Introduction

This section presents the recent developments concerning the global implementation of the GPD algorithm.

Several changes had to be made to the program in order to handle properly global data sets.

Initially, to reduce the amount of data involved in the processing of Envisat global data files, only coastal data were used, by selecting data in a coastal band of 300 km from the coast. Later, this approach was abandoned, since it was found that an efficient global computation required the use of global files including all ocean data.

1) Envisat data

From the global Envisat data files extracted from RADS, all ocean data were selected. As referred above, Envisat data have been extracted from RADS without applying any rejection criterion, to avoid data loss. Subsequently it was found that, in addition to the use of the radiometer land/ocean (MWR_LO) and the radiometer quality interpolation (MWR_Qual) flags, the MWR measurements required additional rejection criteria, in order to detect noisy measurements, mostly contaminated by rain or ice. This was done by creating an MWR rejection flag (MWR_REJ) according to the following criteria:

- MWR_REJ = 1 – if the MWR_LO flag is 1
- MWR_REJ = 2 – if the MWR_Qual is $\neq 0$
- MWR_REJ = 3 – if the ice flag is 1
- MWR_REJ = 4 – if the MWR wet tropospheric correction is ≥ 0 or < -0.5 m.
- MWR_REJ = 5 – if the absolute value of the difference between the MWR and ECMWF wet tropospheric corrections is ≥ 10 cm.

In summary, an MWR measurement is considered valid whenever none of the above conditions occur, that is, when MWR_REJ is 0. In all other cases the point is considered to have an invalid MWR correction and being thus a point for which the correction is to be estimated by the GPD algorithm.

Figure 21 illustrates, for Envisat cycle 68, the points for which the MWR_REJ flag is not zero, that is, the points where new values of the wet tropospheric correction will be estimated. This figure shows that in this implementation, the GPD is not a coastal algorithm anymore. It is an ocean algorithm, including open ocean, high latitudes and coastal zones.

2) ECMWF

From ECMWF global grids containing 721 × 1 440 = 1 038 240 points, data were selected as follows: over ocean all points are selected; over land only points up to 30 km from the coast(Figures 22 and 23). The reason for using more ocean than land data is because we wish to reduce the influence of land data in the estimation to the minimum to warrant that all points will have available ECMWF data for the computation. The total number of ECMWF points used is 713 367, which reduces the data to 69% of the initial size.

For each grid point, the ZWD was computed at the ECMWF orography level, from the parameters TCWV and T_0, according to (5) and (6) and, only for land points, further reduced to sea level according to (7).

3) GNSS data

Data from 190 stations were used, processed as described in the previous sections in order to get ZWD at sea level.

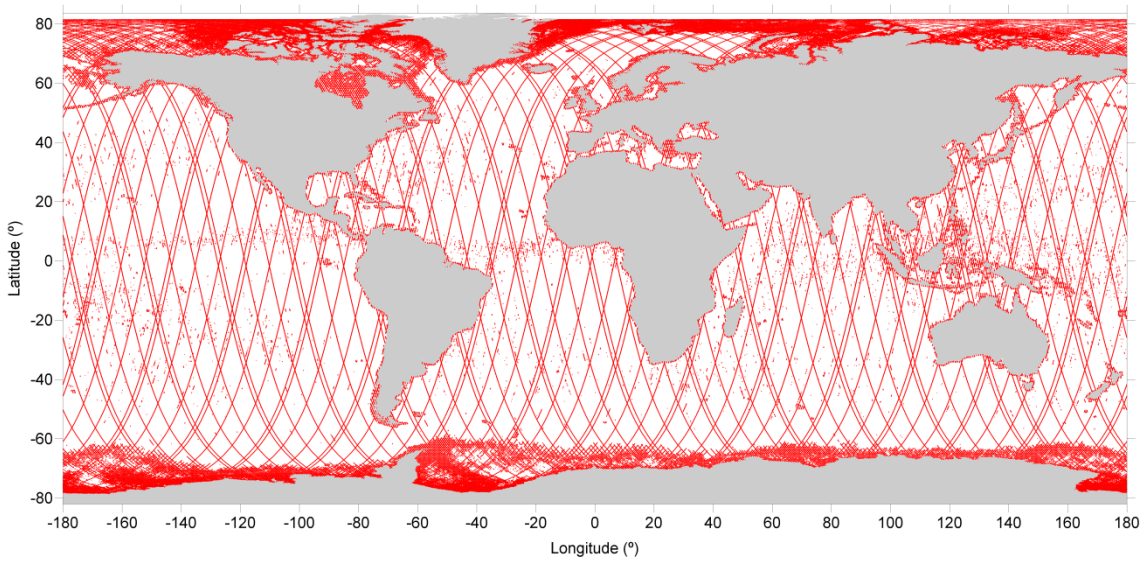

Fig.21 – Location of Envisat cycle 58 points selected for the GPD computation. Only points with invalid MWR data (MWR_REJ ≠ 0) are shown.

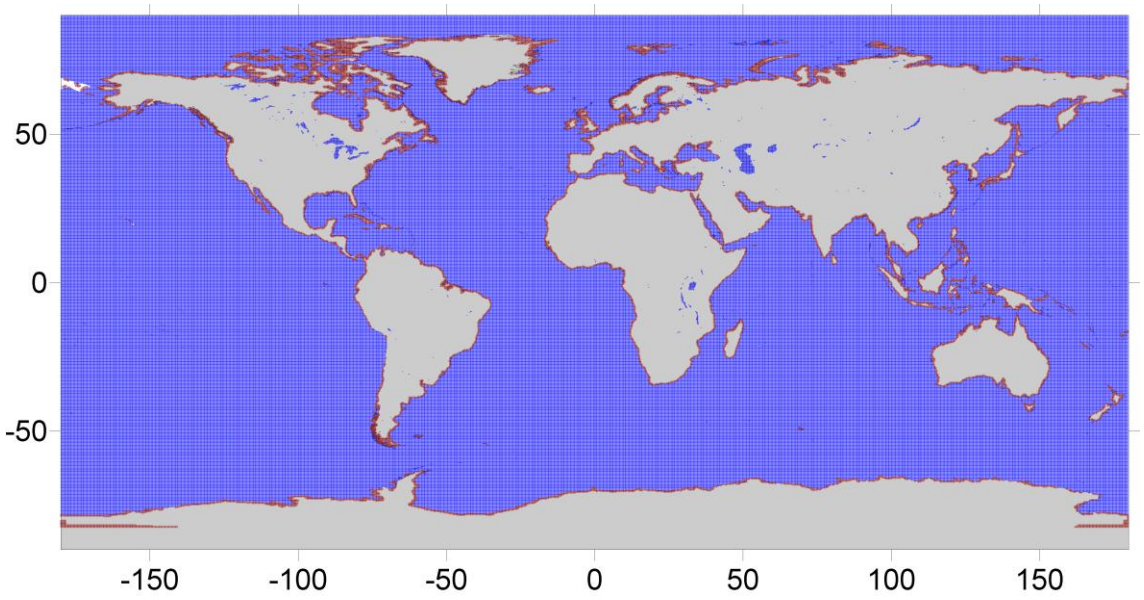

Fig.22 – Location of ECMWF grid points selected for the GPD computation. blue – points over ocean; brown – points over land up to 30 km from the coast.

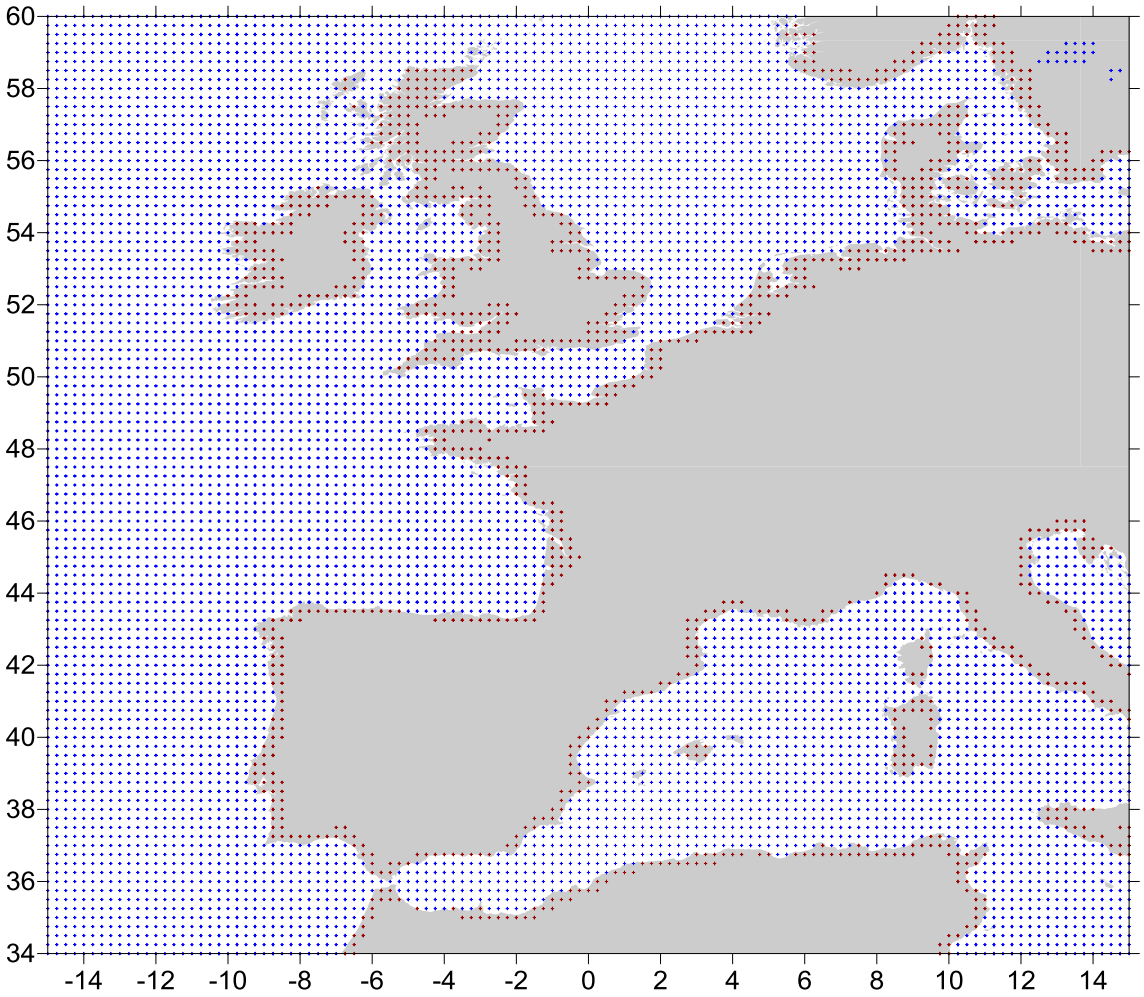

Fig.23 – Location of ECMWF grid points selected for the GPD computation in the European region. blue – points over ocean; brown – points over land up to 30 km from the coast.

Various minor but laborious changes were introduced to the algorithm. Most of them were related to the adequate handling of global data, such as appropriate data treatment at the longitude boundaries, efficient way to compute the distances between points, etc.

The algorithm is run for each satellite cycle. For this purpose, prior to run the algorithm and to reduce the amount of data to be handled, GNSS data are separated into files spanning the period of each Envisat cycle. Concerning MWR data, all ocean points spanning one entire cycle are input. Each ECMWF grid is read only when required, as the processing is progressing.

As presented on Deliverable D2.1d we presently adopted for the spatial correlation function of the ZWD field a Gaussian function with the following scale factor: 100 km for all latitudes in the band |latitude| $\leq$ 55° and 70 km for |latitude| > 55°.

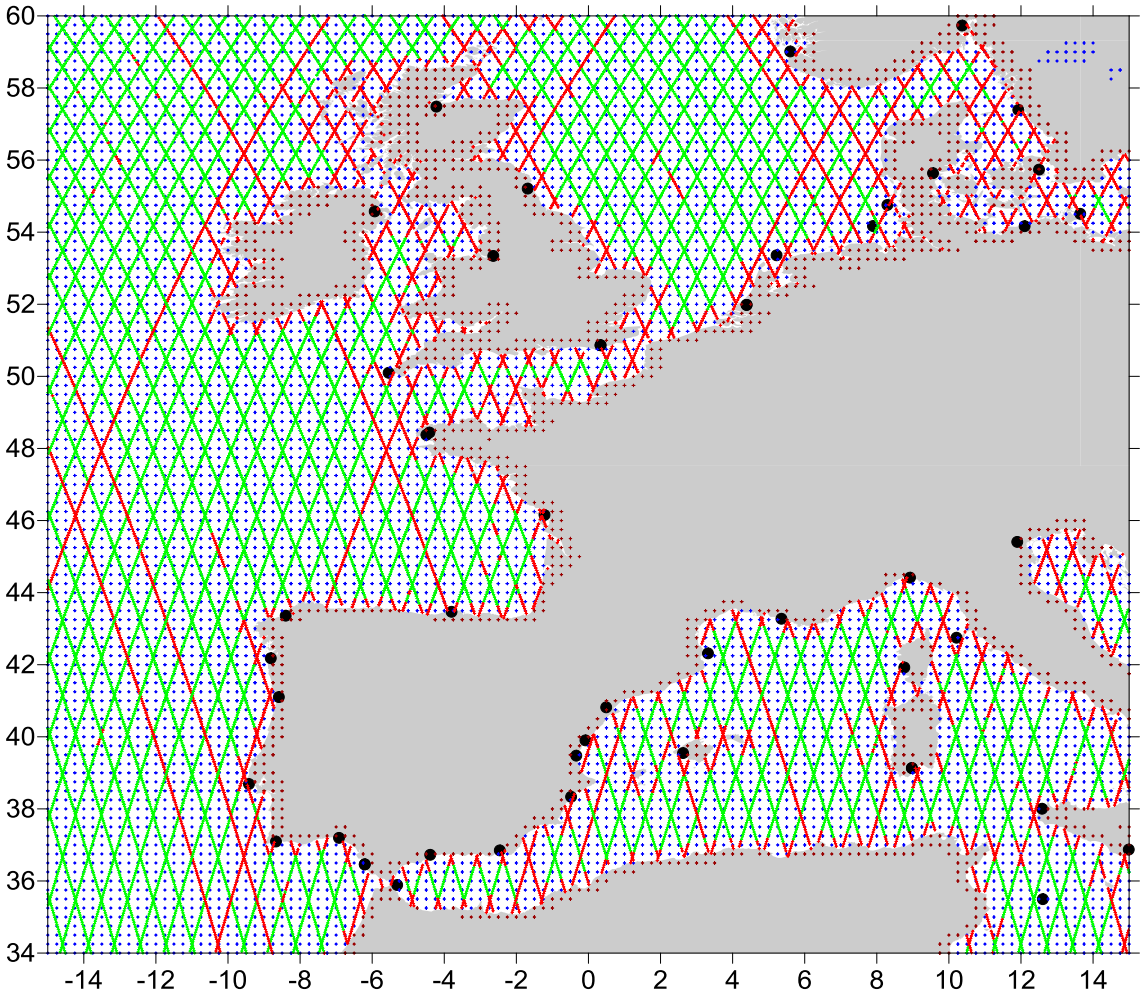

Fig.24 – Location of all data sets selected for the GPD computation. blue – ECMWF points over ocean; brown – ECMWF points over land up to 30 km from the coast; green – Envisat points with valid MWR data; red – Envisat points with invalid MWR data (see text for details); black – GNSS stations.

3.2 Results

The output of the algorithm for Envisat cycle 58 is illustrated in this section. Figure 25 shows the global distribution of the GPD formal error, while Figure 26 shows an enlarged version of the previous plot for the Indonesian region. The results are very similar to those presented in Fernandes et al. (2010).

To understand these maps we have to recall that the GPD error is a function of the spatial and temporal distribution of the observations relative to the point of computation and also on the signal variance on the same point. The orange and brown tracks with larger errors are passes with all MWR measurements invalid. In this case the only available data for the algorithm is ECMWF which can be at a time difference with respect to the satellite measurements up to 3 hours. Comparing these maps with the map of the standard deviation of the ZWD field shown in Figure 6 it can also be observed that, as expected, the largest errors are located in regions of large field variance.

Figures 27 to 29 illustrate the wet GPD output for Envisat cycle 58. In Figures 28 and 29, the shaded areas indicate regions where the mwr_rejection_flag (MWR_REJ, in grey) or the GPD_interp_flag (GPD_INT, in green) were set. The first refers to the locations identified by the algorithm as requiring an estimation; the later refers to the locations for which the algorithm acted successfully. The absence of grey areas in the plots indicates that in these tracks all points possess a valid estimate.

Apart from the algorithm performance in the coastal regions, which has already been shown on previous reports, these plots illustrate the performance of the algorithm at the high latitudes, where the MWR measurements are contaminated by ice. Here, the correction will be dominated by the ECMWF model, improved by the GNSS data near the coast, where available.

At present the algorithm is successfully running globally providing sensible estimates in all altimeter ocean points. All points for which there is a valid GPD estimate are attributed the value 1 to the corresponding flag (GPD_interp_flag). Only a few number of points remain for which the algorithm returns a somehow unexpected value and have been properly flagged (GPD_interp_flag=3). This behaviour seems to be related with locations for which the observations possess very close points with relatively large variations. In addition, since the ECMWF land/sea mask does not coincide with the altimeter land/ocean flag, a very small number of points exist for which there are no data for the estimation (GPD_interp_flag=2). Figure 30 illustrates the GPD_interp_flag for all points where the algorithm attempted to compute an estimate (439 753 points). From these points, 303 (0.06%) have an unexpected estimate (GPD_interp_flag=3) and for 75 (0.02%) there were no data for the estimation (GPD_interp_flag=2).

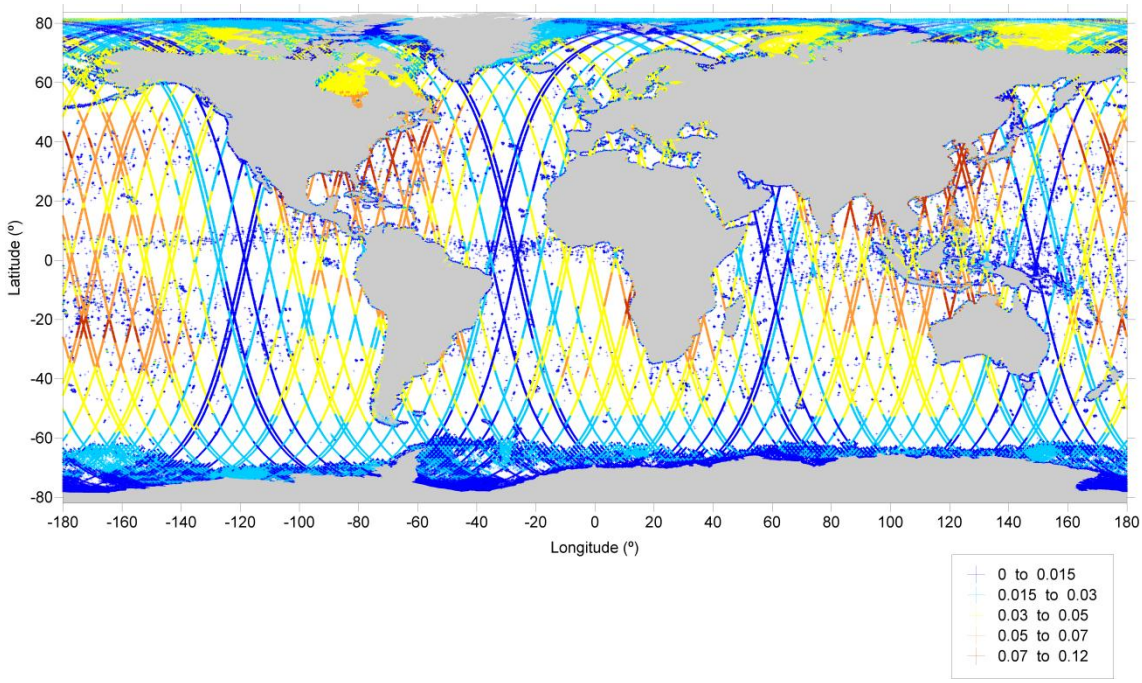

Fig.25 – Formal error (in metres) for Envisat cycle 58.

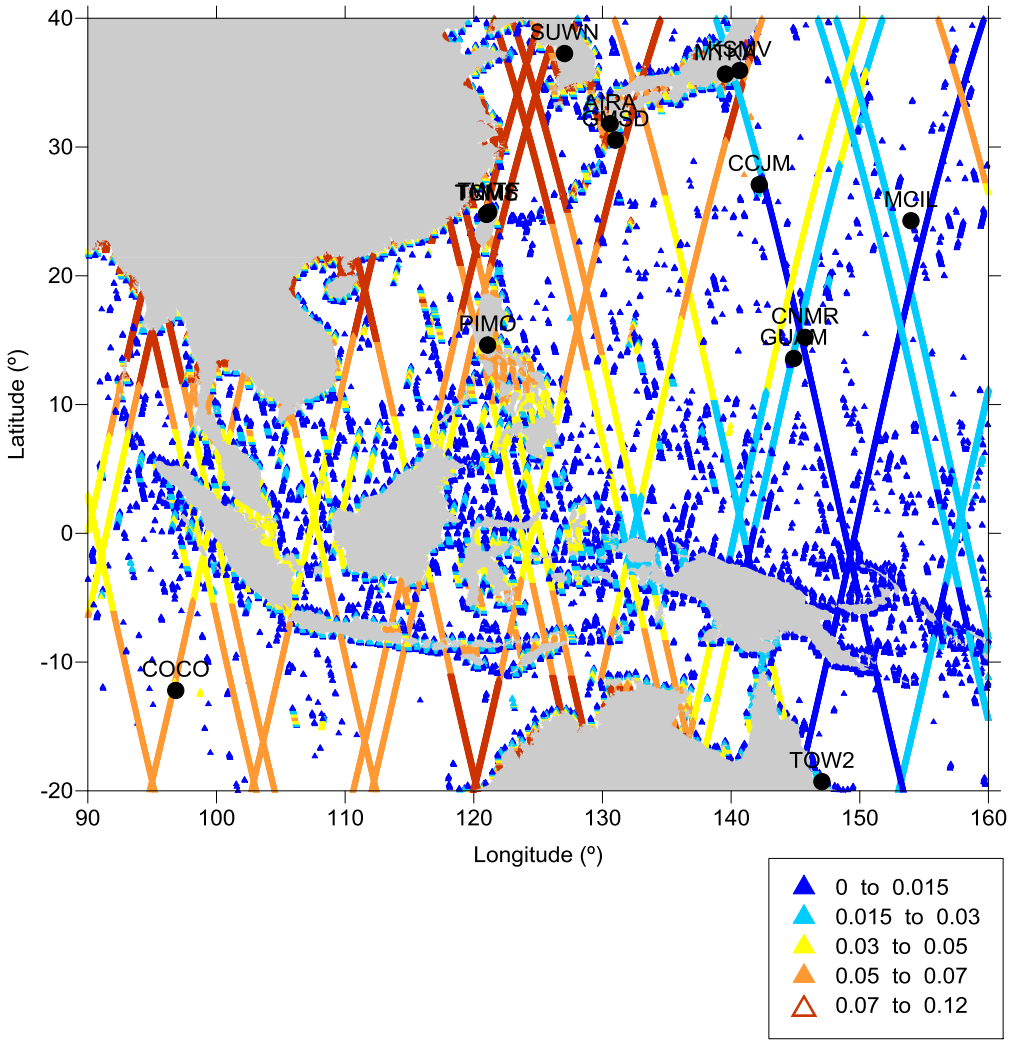

Fig.26 – Formal error (in metres) for Envisat cycle 58, for a region around Indonesia.

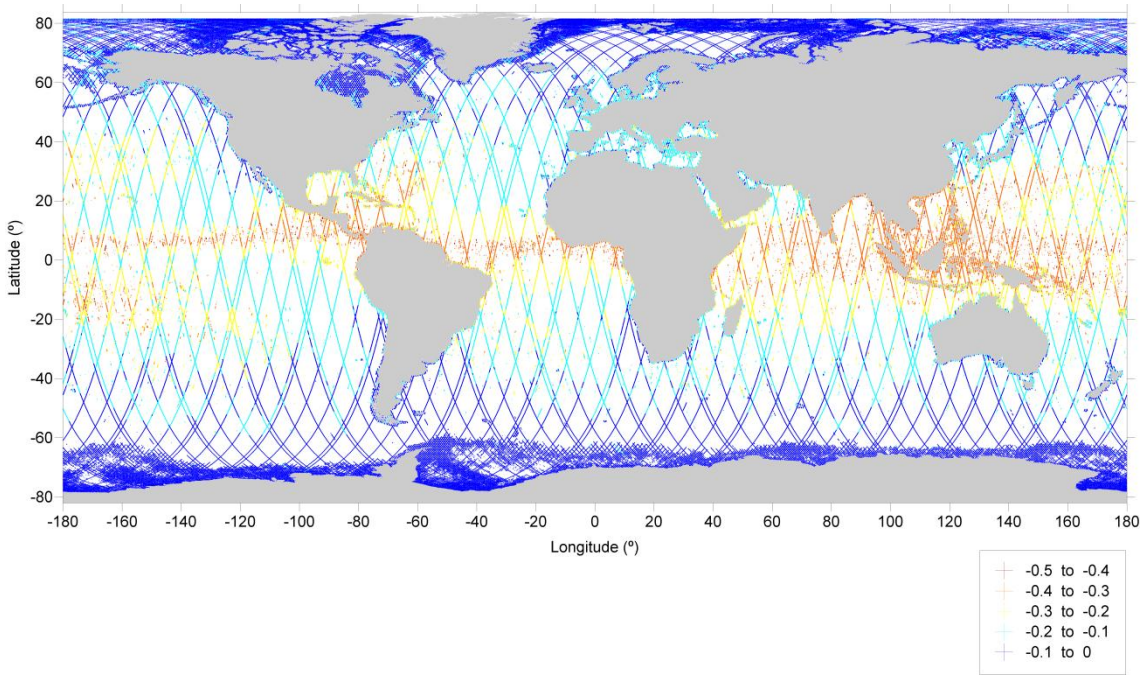

Fig.27 – Estimated GPD wet tropospheric correction (in metres) for Envisat cycle 58.

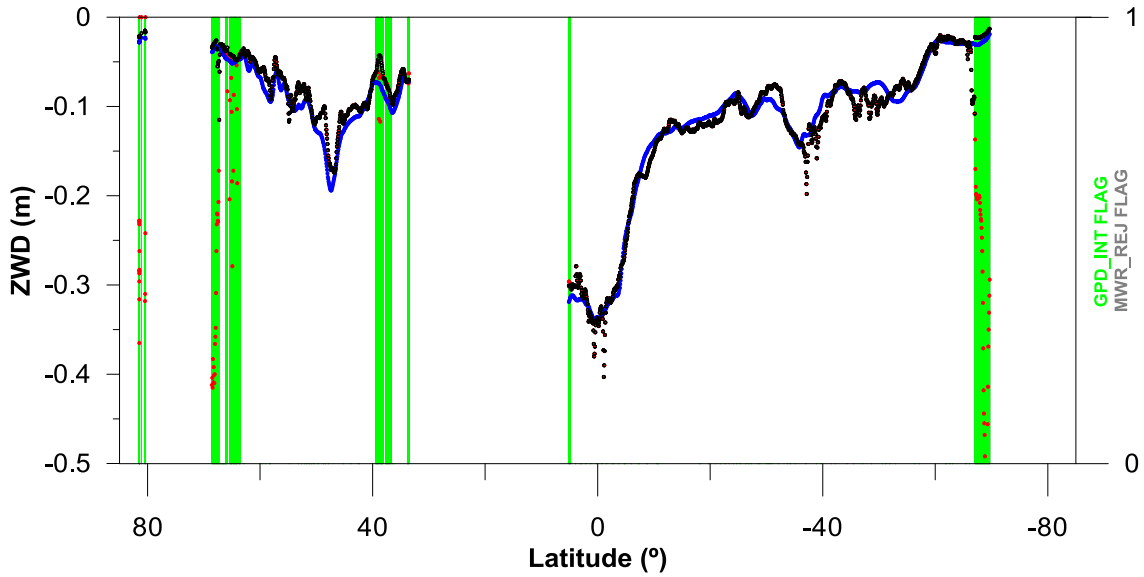

Fig.28 – Results obtained for Envisat pass 001 cycle 58. The wet tropospheric correction from three data sets is shown (in meters): MWR (red), ECMWF-model from GDR (blue) and GPD output (black). The shaded areas indicate regions where the MWR_REJ flag (grey) or the GPD_INT Flag (green) were set.

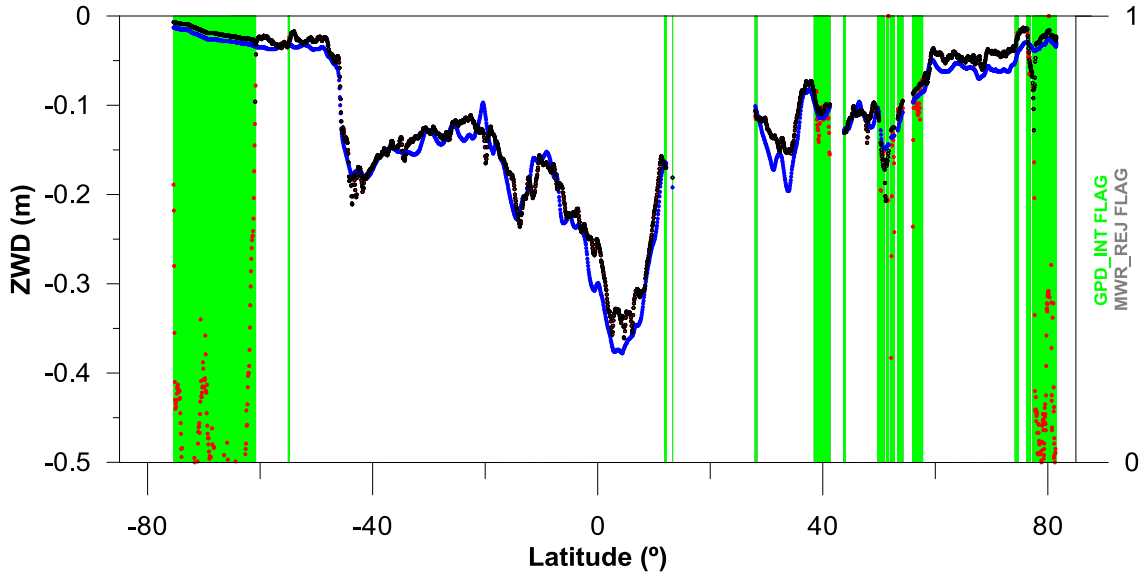

Fig.29 – Same as on Fig. 28 for Envisat pass 160 cycle 58.

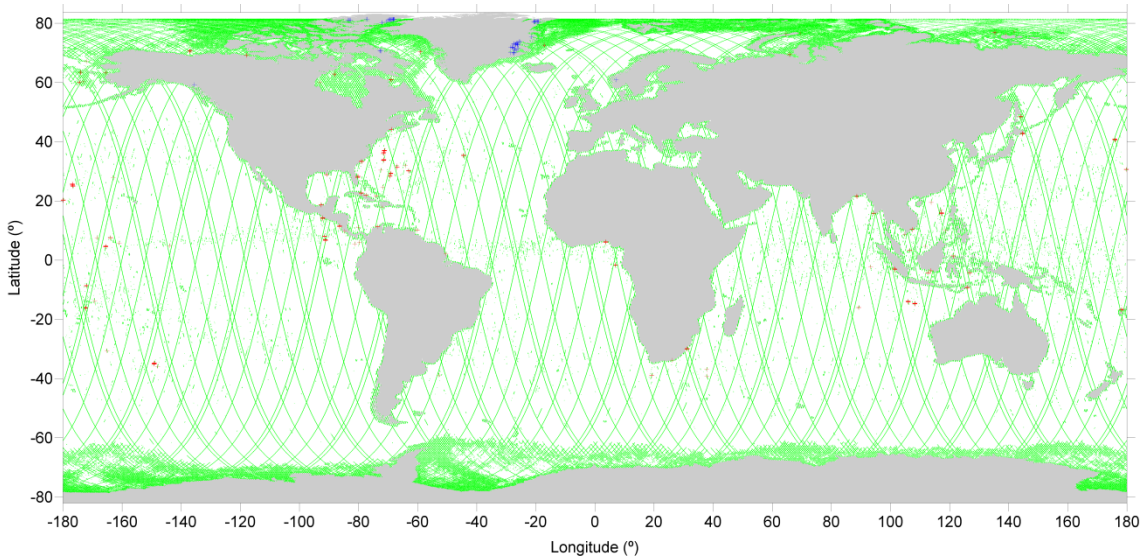

Fig.30 – Representation of the GPD_interp_flag for Envisat cycle 58: green: points with GPD_interp_flag=1; blue: points with GPD_interp_flag=2; red: points with GPD_interp_flag=3 (see text for details).

3.3 Description of GPD output fields

The data are provided at 1Hz ASCII files, containing all data points within the 300 km coastal band represented in Figure 22.

Each file contains the following fields:

cycle

pass

MJD

Latitude
Longitude
dry_ tropo_corr
mod_wet_ tropo_corr
mwr_wet_ tropo_corr
altim_landocean_flag
mwr_rejection_flag
GPD_wet_tropo_cor
GPD_interp_flag
GPD_formal_error
GPD_num_ponts
GPD_signal _variance

Field description:

All fields are as described in the GDR and COASTALT manuals. Here only the new fields are described:

mwr_rejection_flag

- 1 – if MWR_LO = 1
- 2 – if MWR_Qual $\neq$ 0
- 3 – if the ice flag is 1
- 4 – if mwr_wet_ tropo_corr $\geq$ 0 or mwr_wet_ tropo_corr < - 0.5 m.
- 5 – if | mwr_wet_ tropo_corr - mod_wet_ tropo_corr | $\geq$ 10 cm.

GPD_wet_tropo_corr – 1Hz wet tropospheric correction computed as described in section 3 (in metres). This correction is valid when the GPD_interp_flag is 0 or 1.

GPD_interp_flag – 1Hz GPD flag set as follows:

- 0 – ocean points for which the MWR correction is valid. In this case the GPD correction is set as equal to the original MWR correction
- 1 – points for which the GPD algorithm provided a valid output
- 2 – points for which there were no data points to compute the GPD correction
- 3 – points for which the algorithm outputs an unexpexted estimate, according to algorithm internal criteria

For all cases except when the above flag is 1, fields GPD_formal_error and GPD_signal_variance are set to a default value of 9.000 and field GPD_num_points is set to 0.

GPD_formal_error – Formal error in the GPD estimation (in metres)

GPD_num_ponts – Number of data points (of any data type) used in the GPD estimation

GPD_signal _variance – signal variance in m^2.

Note that although the field related with the dry tropospheric correction has been mentioned as an input field of the GPD program and is also provided in the GPD 1Hz files, actually this field is not used in the GPD estimation. It is only provided for completeness, since it is a useful field for various studies.

4 Conclusions

Summary of the main conclusions presented in this study:

- There is a very good agreement between the ZWD derived from the GNSS path delays and the corresponding value determined from ECMWF. The mean difference has an absolute value less than 3 mm and the standard deviation is 13 mm.
- Statistics of the differences between GNSS –derived ZWD with the corresponding MWR-derived wet tropospheric correction at the Envisat nearby points, for a group of 136 stations which were considered to have enough data for the comparison, is: 0.93, -5.8, 20.0 mm for the correlation, mean and standard deviation respectively.
- These results indicate that the methodologies for handling GNSS and ECMWF data seem to be appropriate. No evidence of systematic errors in the GNSS stations was found.
- A surprising result was the problems found in the MWR measurements which usually are considered the most accurate method to determine the wet tropospheric correction. Overall this study shows that the inter-comparison of various data sets provides a lot of information and gives further insight about the strengthens and weakness of each measurement technique.

- The above results also show that it is very important to use adequate methods to filter the noisy MWR data prior to run the GPD algorithm since noisy measurements will corrupt the estimation of the nearby points.
- A global implementation of the GPD algorithm is presently running at UPorto enabling the computation of the wet tropospheric correction, everywhere over ocean, including the coastal areas and the high latitude regions. The correction is continuous with respect to the original MWR correction, replacing this one whenever a point is considered to have an invalid MWR value. Only a few points (less than 0.1%) remain with estimates that are somehow unexpected, for which a close inspection is desirable. At present, these measurements have been properly flagged as invalid estimates.

Acknowledgements

The authors would like to acknowledge the European Centre for Medium Range Weather Forecasts (ECMWF) for providing the reanalysis data on the single-level atmospheric fields of the Deterministic Atmospheric Model.

The authors would also like to acknowledge Radar Altimeter Database System (RADS) for providing the altimetric data and very gratefully thank Remko Scharroo (NOAA / Altimetrics LLC) for his prompt help and precious information about the data details for the various altimeters.

References

Askne, J. and H. Nordius, (1987) Estimation of tropospheric delay for microwaves from surface weather data, Radio Sci., vol. 22, pp. 379–386.

Boehm J, Niell A, Tregoning P, Schuh H (2006) Global Mapping Functions (GMF): a new empirical mapping function based on numerical weather model data. Geophysical Research Letters 33(L07304) doi:10.1029/2005GL025546

Boehm J., and H. Schuh (2004) Vienna mapping functions in VLBI analyses, Geophys. Res. Lett., vol. 31, L01603,

Dach R, Hugentobler U, Fridez P, Meindl M (Eds.) (2007) Bernese GPS Software - Version 5.0. Astronomical Institute, University of Bern

Davis JL, Herring TA, Shapiro II, Rogers AEE, Elgered G (1985) Geodesy by radio interferometry: effects of atmospheric modelling errors on estimates of baseline length. Radio Science 20(6):1593-1607

ECMWF (2009) http://www.ecmwf.int/products/catalogue/pseta.html

Fernandes M. J., C. Lázaro, A. L. Nunes, N. Pires, L. Bastos, V. B. Mendes (2010) GNSS-derived Path Delay: an approach to compute the wet tropospheric correction for coastal altimetry, IEEE Geosci. Rem. Sens Lett., in press

Herring T, King R, McClusky S (2006) GAMIT Reference Manual – GPS Analysis at MIT - Release 10.3. Department of Earth, Atmospheric and Planetary Sciences, Massachusetts Institute of Technology

Kouba J. (2008) Implementation and testing of the gridded Vienna Mapping Function 1 (VMF1). Journal of Geodesy 82:193-205 doi:10.1007/s00190-007-0170-0

Kouba, J. (2009) A guide to using International GNSS Service (IGS) Products. Geodetic Survey Division, Natural Resources Canada

Mendes, V. B., G. Prates, L. Santos, and R. B. Langley, “An evaluation of the accuracy of models of the determination of the weighted mean temperature of the atmosphere”, in Proc. ION 2000 National Technical Meeting, Anaheim, CA.

Niell, A.E. (2001) Preliminary evaluation of atmospheric mapping functions based on numerical weather models. Physics and Chemistry of the Earth 26:475–480

Ray, R. D. (1999) A Global Ocean Tide Model from TOPEX/POSEIDON Altimetry: GOT99.2. NASA Technical Memorandum 209478

Zumberge, J.F., Heflin, M.B., Jefferson, D.C., Watkins, M.M., and F.H. Webb, (1997), Precise point positioning for the efficient and robust analysis of GPS data from large networks. J. Geophys. Res., 102, 5005-5017.